R & M No.3817

R & M No.3817

PROCUREMENT EXECUTIVE, MINISTRY OF DEFENCE

Aeronautical Research Council
Reports and Memoranda

FATIGUE ACCELERATION IN BOX BEAMS UNDER MECHANICAL AND THERMAL STRESS

(Second Series)

by

F.E. Keates, F.E. Kiddle, R.F. Mousley and D. Gunn

Structures Department, RAE Farnborough

LIBRARY
ROYAL AIRCRAFT ESTABLISHMENT
BEDFORD

London: Her Majesty's Stationery Office
1978

PRICE £6 NET

FATIGUE ACCELERATION IN BOX BEAMS UNDER MECHANICAL AND THERMAL STRESS

(Second Series)

By F.E. Keates, F.E. Kiddle, R.F. Mousley and D. Gunn

Structures Department, RAE Farnborough

Reports and Memoranda No.3817*

July 1976

SUMMARY

To assist the development and interpretation of the Concorde Major Fatigue Test a technique for accelerating fatigue testing was evaluated on structural box specimens under combined mechanical and thermal loadings.

It is shown that for a moderate level of thermal fatigue the acceleration achieved was in reasonably good agreement with prediction but that at a high level of thermal fatigue the acceleration was appreciably higher than predicted. A tendency was observed for acceleration to be higher in crack propagation than in crack initiation.

* Replaces RAE Technical Report 76096 - ARC 37369

CONTENTS

1 INTRODUCTION

In order to meet certification requirements within an acceptable time-scale the accumulation of fatigue damage by an aircraft structure subjected to a full scale fatigue test must be faster than in operational service.

In the case of subsonic aircraft, where only the mechanical loading is significant in fatigue, the main method of accelerating the test is to omit from the loading sequence all periods when the aircraft is under steady load. However, a supersonic aircraft is subject not only to mechanical loading but also to thermal loading which gives rise to transient temperature gradients through the structure. Associated with these temperature gradients are thermal stresses which make a significant contribution to fatigue damage. The thermal cycle also results in the aircraft being at elevated temperature during supersonic cruise when time dependent effects such as creep and over-ageing can occur. Therefore in order to simulate the effects of the thermal cycle in full scale fatigue tests and to maintain an acceptable degree of acceleration a new approach is required.

To assist the development and interpretation of the Concorde Major Fatigue Test (CMFT)[1] an experimental investigation was carried out at RAE in collaboration with BAC into the acceleration of fatigue in structural box specimens under the combined action of mechanical and thermal stresses. The first series of tests[2] established the broad feasibility of accelerating the test by the technique of reducing the number of thermal cycles applied but increasing the temperature range and hence the thermal stress amplitude. The second series of tests reported here provided more refined simulations of conditions in service and in test, particularly in the representation of temperature levels, of dwells at elevated temperature, and of the relative proportions of thermal and mechanical fatigue damage.

In the Report, acceleration factors are calculated as the ratio of the fatigue lives of specimens under unaccelerated and accelerated loadings and are assessed by comparing test values with those predicted by various methods.

2 SPECIMEN

The specimens were fabricated boxes approximately 16in square and 10ft long constructed mainly from CM001 (clad RR58) sheet. They were designed and manufactured to standards for Concorde fuselage structure but were not intended to represent a specific part of the aircraft. The depth of the specimen was chosen so that significant thermal stresses developed when the flanges (top and

bottom panels) of the specimen were heated or cooled relative to the shear webs (side panels) at rates similar to those which occur in the CMFT and in Service.

Fig.1 is a general diagram of the box specimen which was of riveted skin-stringer construction. Z-section stringers supported the skin panels of the curved compression flange and of the shear webs, while flanged T section stringers supported the skin panel of the tension flange. Detail drawings of the specimen are shown in Figs.2 to 5. In this investigation the feature of particular interest was the Monel riveted butt strap joint midway along the tension flange of the specimen (see Fig.2).

Each specimen was instrumented with strain gauges, platinum resistance thermometers and thermocouples so that thermal and mechanical stresses and temperature distributions could be measured. The instrumentation was located at the stations defined in Fig.6. The temperature of each box was controlled from the platinum resistance thermometers positioned at Station C. The temperature distribution at this section was considered to give a good measure of the average temperature and temperature differential along the length of the box and therefore the best indication of the thermal stress at the butt strap joint. By contrast, temperatures at the joint were subject to local lag due to the mass of the joint members and were not an accurate reflection of local thermal stress conditions.

The construction and instrumentation of the specimens are described more fully in Appendix A.

3 TESTING RIG

The function of the testing rig was to apply a programme of loads and temperature to the specimen which was loaded mechanically in four point bending and was heated and cooled by convection from air passed over its surfaces. The general arrangement of the rig is shown in Fig.7 and a description of the rig and its operation is given in Appendix B.

Thermal stresses were induced in the specimen by heating or cooling the flanges relative to the shear webs and a mechanical system of hydraulic jacks, control valves and control gauges applied the mechanical loads. The thermal system consisted of two insulated duct systems, one to heat and cool the webs and the other to heat and cool the flanges (see Fig.7). The two duct systems were isolated from each other and were each connected to re-circulation circuits. Heat was obtained from banks of 1kW commercial fire bars positioned in the

ducting upsteam of the specimen and the coolant was a mixture of air and liquid nitrogen controlled to cool the specimen at a predetermined rate.

4 TESTING

The programme of testing was designed to investigate the acceleration of fatigue in the butt strap joint on the tension flange of the box beam specimens. Twelve specimens (numbered 13 to 24) were tested using simple flight-by-flight load and temperature sequences based on those experienced by the Concorde wing structure.

Four different sequences were used, two of which were based on aircraft service loadings (designated Service) and two were based on accelerated loadings typical of the Concorde Major Fatigue Test (designated CMFT). Three specimens were tested under each of the four load and temperature sequences. Occasionally during each test the temperature and stress variations at many positions on the specimen were monitored during a complete load and temperature sequence.

The Service temperature sequences were simple representations of the conditions experienced by the aircraft wing during a typical supersonic flight (see Fig.8). The mechanical loading simulated a ground-air-ground cycle and included a period of steady load representing the cruise followed by a number of constant amplitude gust cycles. The number of gusts and the levels of mechanical loadings were established to give a predicted specimen life of about 10000 cycles (i.e. about three years) while restricting the peak tensile stresses to reasonably realistic levels. During the cruise phase of the sequence, thermal stresses were induced in the specimens by first heating and later cooling the flanges relative to the webs thereby representing conditions in deep structure at the beginning and end of supersonic cruise. Two different degrees of thermal stress fatigue damage were investigated and the two Service load and temperature sequences were designed such that either 40% or 80% of the fatigue damage accumulated during each sequence was caused by the thermal stress cycle. These will be referred to as the Service 40 and Service 80 sequences respectively. The two degrees of thermal fatigue damage were achieved by adjusting the thermal stress amplitude and the number of gust cycles applied per sequence as described in Appendix C.

The CMFT load and temperature sequences (Fig.9) were designed to be as fatigue damaging as two of the simplified Service loading sequences, i.e. to achieve an acceleration factor of two with respect to the Service cases. The mechanical loading sequence was the same as for the Service cycle but it was applied twice during each CMFT cycle. The first of these sequences contained a load dwell representing the cruise during which the temperatures of the webs and

flanges were varied in the same way as in the Service cases, but over a greater temperature range. This increased temperature range was chosen with the intention that a thermal stress cycle in the CMFT tests would cause twice as much fatigue damage as a thermal stress cycle in the Service tests. On the basis of S-N data[3] for small bolted joint specimens it was assumed that this would entail an increase in thermal stress amplitude by a factor of 1.28. Before the necessary increase in temperature range could be determined the relationship between thermally induced stress in the flange and the temperature difference between the webs and flanges had to be established for a typical box specimen. Fig.10 shows the results of preliminary tests on one of the boxes and it is seen that this relationship is linear at Station C, the position chosen for controlling the box temperature. Accordingly the maximum and minimum temperatures used in the CMFT cycle were chosen such that the temperature difference between flanges and webs was increased by a factor of approximately 1.28 in both the heating and cooling phases.

In the CMFT tests the cruise period was shorter than in the Service tests and no cruise period or thermal cycle was applied during the second mechanical sequence of each CMFT cycle. As in the Service cases, two load and temperature sequences were designed such that either 40% or 80% of the fatigue damage in each sequence was caused by the thermal stress cycle. These were known as the CMFT 40 and CMFT 80 sequences respectively and were achieved using the same techniques as in the Service cases (see Appendix C).

All tests were interrupted at intervals for crack detection and growth measurements. The area of the butt strap joint was examined using radiographic techniques. In general, fatigue cracks from rivet holes could be detected once they had propagated beyond the periphery of the rivet head, i.e. when they were approximately 0.1in in length. Crack lengths were measured often during each test and in this way records of crack propagation at the joint were obtained.

5 TEST RESULTS

Throughout all tests, temperatures and stresses on the webs and flanges of the boxes were measured at various stations. For each load and temperature sequence typical variations of web and flange temperatures at Station C are given in Figs.11 to 14. The achieved temperatures were generally in good agreement with the nominal values (see Appendix D). Combined mechanical and thermal stresses in the tension flange of each box were measured on the gross section at

Station C and were factored to obtain the average net stress at the butt strap joint. Variations of net stress at the joint during the thermal cycle are shown in Figs.18 to 21 for each of the load and temperature sequences. (Strain gauge and thermocouple readings are not available for boxes 21 and 22.)

During testing the butt strap joint was the only location at which fatigue cracking occurred in all specimens. Two stages of fatigue damage were most readily identified in each specimen, the first crack and final failure. The first crack is defined as the earliest crack detected by radiographic examination and was about 0.1in long (see section 4); at final failure cracking was so widespread that most of the load was carried in the boom angles at the joints between the tension flange and shear webs. Damage locations for all tests are given in Table 1 and crack growth is shown diagrammatically in Figs.22 to 33. It is seen that first crack and final failure always occurred at the most heavily loaded sections, i.e. damage in the butt strap and stringers occurred at either rivet row C or rivet row D and damage in the skin and stringers occurred at either rivet row A or rivet row F, although final failure was not always through the rivet row in which the first crack appeared. An analysis of crack growth characteristics is given in Appendix E. The lives to each stage of crack growth were recorded for all tests and these results are given in Table 1 with estimates of log mean lives. Box 13 was subjected to certain irregularities during production and instrumentation and it was used for preparatory testing prior to the main test programme. It was therefore considered unrepresentative and although the test results for this box are given in Table 1, they were not used in the estimation of log mean life.

A statistical analysis of the test results was carried out using the method given in Appendix F. The estimated variance of the log mean fatigue lives to first crack and to failure were 0.00191 and 0.00288 respectively. These values are compatible with constant amplitude fatigue of riveted aluminium alloy structure at about 10^4 cycles.

At intervals during testing the deflections of specimens due to creep were measured. The method used was not very accurate and there was considerable scatter in the results. Permanent deflections developed during most tests but no consistent trend was discernible for any group of tests. The measurements indicated that overall creep strains were small, the maximum being approximately 9×10^{-5} at the tension flange. In addition, when the fracture surfaces of some specimens were studied (Appendix E) they displayed no characteristics associated

with creep cracking. From these results it was concluded that the overall creep during these tests was insignificant.

6 PREDICTION OF SPECIMEN FATIGUE LIVES AND ACCELERATION FACTORS

The predictions of the fatigue lives of specimens under the four load and temperature sequences were based on stress levels measured during testing (Figs.18 to 21). The stresses measured on specimens subjected to nominally the same loading were averaged and a mean stress sequence was obtained for each condition.

The fatigue lives were evaluated using both the Separate Cycle and Range Mean Pair methods of stress sequence analysis, each in conjunction with Miner's cumulative damage law (see Appendix G). Two sources of S-N data were used in the life prediction, the BAC Structural Design Data for typical light alloy aircraft joints[3] (Fig.36) and the BAC Standard Curve Equation[5], and there was no allowance for possible effects of elevated temperature on fatigue behaviour.

Each method of stress sequence analysis was used in conjunction with each set of S-N data and hence four predictions of the fatigue life were obtained for specimens tested under each load and temperature sequence. Values of acceleration factor were calculated by comparing predicted fatigue lives of specimens tested under Service loadings with those of specimens tested under CMFT loadings. The results are summarised in Table 3.

In the Separate Cycle Method of analysis the complete stress sequence was divided into its separate components, i.e. ground-air-ground cycle, thermal stress cycle and gust loading cycles. Therefore with this method it was possible to calculate the proportion of the total fatigue damage which was caused by the thermal stress cycle for each load and temperature sequence and these values are also given in Table 3.

7 DISCUSSION

Acceleration factors were calculated from the test results by four methods which are distinguished by the way in which first crack and failure are defined (see Appendix H). The values calculated by the different methods are presented in the following table together with the values predicted from S-N data as described in section 6.

Nominal proportion of damage due to thermal fatigue (%)	Stage of damage	Test acceleration factor (for methods see Appendix H)				Predicted acceleration factor			
						Separate Cycle Method		Range Mean Pair Method	
		A	B	C	D	L.A. aircraft joints data	Standard Curve Equation	L.A. aircraft joints data	Standard Curve Equation
80	1st crack	2.7	2.7	3.0	2.5 or 2.7				
	Failure	3.1	2.9	3.1	3.0 or 3.7	1.8	2.1	1.8	2.1
40	1st crack	2.2	2.2	2.4	2.2				
	Failure	2.5	2.4	2.5	2.7 or 2.2	2.0	2.4	2.0	2.4

It is seen that the test acceleration factors based on log mean lives do not vary markedly with the method of calculation, the general variation being less than 10%.

It is concluded that the method chosen to interpret the test results is not critical.

In all cases test acceleration factors to failure are greater than those to first crack suggesting that the more advanced stages of crack propagation were accelerated more than crack initiation and early crack growth.

The table also shows that the predicted acceleration factors calculated by the two methods of stress sequence analysis were the same (see Appendix G). Furthermore, the values differed only by about 15% for the two sets of S-N data. It is seen therefore that, in these cases, predicted acceleration factors do not vary significantly with the method of calculation.

Comparison of the predicted acceleration factors with those achieved by test shows that in cases where nominally 80% of the fatigue damage was caused by the thermal stress cycle, the test acceleration factors were always higher than predicted values. In the 40% cases, agreement between the test and predicted

values was quite good. These results are in agreement with those of the earlier work[2] and show that the acceleration techniques used give reasonably predictable results in these more representative tests.

8 CONCLUSIONS

Tests have been carried out to study the acceleration of fatigue in structural box beam specimens under flight-by-flight sequences of mechanical and thermal stresses. The sequences were designed to represent two levels of thermal fatigue which occur in the Concorde aircraft. The following conclusions were reached:

(a) Under combined mechanical and thermal stresses, the accumulation of fatigue damage was accelerated with a reasonable degree of predictability for a moderate level of thermal fatigue but was accelerated more than predicted for a high level of thermal fatigue.

(b) Acceleration to failure was higher than to first crack suggesting that advanced crack propagation was accelerated more than crack initiation and early crack growth.

Appendix A

TEST SPECIMENS AND ATTACHED TRANSDUCERS

The specimens used in this investigation were fabricated boxes, mainly constructed from CM001 sheet (clad RR58 material) and were approximately 16in square and 10ft long. They were designed and manufactured to standards for Concorde fuselage structure although it was not intended to represent a specific part of the aircraft. The depth of the specimen was chosen so that significant thermal stresses developed when the flanges (top and bottom panels) were heated or cooled relative to the shear webs (side panels) at rates similar to those which occur in the CMFT and in Service.

Fig.1 is a general diagram of the box specimen which was of skin-stringer construction. Before assembly of the box, all parts were cleaned and then painted with one coat of barium chlorate primer ICI F580/2022. All joints were assembled with Viton fluorocarbon polymer interfay which was allowed to cure at room temperature. Detail drawings of the specimen are shown in Figs.2 to 5. Flanged T-section stringers supported the skin panel of the tension flange (Fig.2) while Z-section stringers supported the skin panels of the curved compression flange (Fig.3) and of the shear webs (Fig.4). The shear web assembly had four loading attachments so that the box could be loaded in four point bending. Detail drawings of the loading attachments are given in Fig.5. In this investigation the feature of particular interest was the Monel riveted butt strap joint midway along the tension flange of the specimen (see Fig.2).

Each box was instrumented with strain gauges, platinum resistance thermometers, and thermocouples at various stations along the box which are defined in Fig.6. The temperature of each box was controlled from the platinum resistance thermometers positioned at Station C and temperature was monitored from thermocouples attached at each station along the longitudinal centrelines of the webs, compression skin and tension skin. Strain gauges were attached to the flanges and one shear web of each specimen at Stations A, B, C and D. The first box tested (No.13) was more extensively instrumented than other specimens so that the relationship between the induced thermal stress in the flanges and the difference between web and flange temperatures could be established for positions remote from the joint. This relationship was then used to determine the temperature ranges for the accelerated tests. The additional instrumentation consisted of strain gauges and thermocouples attached at various positions across the flanges and one shear web of the box at Stations A, B, C and D.

Appendix B

DESCRIPTION AND OPERATION OF TESTING RIG

The function of the testing rig was to apply a programme of bending loads and temperature to the specimen. The specimen was loaded mechanically in four point bending and it was heated and cooled by convection from air passed over its surfaces. The general arrangement of the rig is shown in Fig.7.

The specimen was supported in the rig by two 'A' frames which in turn were mounted on reaction beams. One 'A' frame was free to move along the longitudinal axis of the rig so that the thermal expansion and contraction of the specimen was unrestricted. Low friction hydraulic jacks applied upward loads at the corners of the specimen to produce uniform bending in the centre section of the box. Bending of reverse sign was produced by a single hydraulic jack at each end of the specimen, pulling down on the loading points. The different load levels called for during one complete flight cycle were controlled by electro-mechanical selector valves; the rate of loading was governed by the hydraulic pump output and specially developed pressure relief valves. During mechanical fatigue cycling, the amplitude of the loads was controlled by Budenberg Max-Min electrical contact pressure gauges; all loads applied were within ±1% of nominal. The complete mechanical loading programme was regulated by a Post Office type uniselector switch and associated relay logic.

The mechanical loads applied to the specimen were calibrated against a Macklow-Smith hydraulic load cell which was checked against a secondary standard. The pressure in the hydraulic loading system was checked daily, and at intervals throughout the test the loads applied to the specimen were rechecked against the load cell. Pressure switches, pressure relief valves and deflection limit switches were incorporated in the rig in order to protect the specimen against overload.

Thermal stresses were induced in the specimen by heating or cooling the flanges of the specimen relative to the shear webs. The insulated duct system over the specimen was divided by flexible membranes of aluminised asbestos cloth and the divisions were connected to separate re-circulation circuits as indicated in Fig.7. Each circuit was equipped with a centrifugal fan, a source of heat input, a liquid nitrogen injection system and a system of flaps to provide either open- or closed-loop operation. The heating sources were banks of 1kW commercial fire bars positioned in the ducts upstream of the specimen and

cooling was by mixtures of ambient air and liquid nitrogen. Temperatures at various positions in the specimens were monitored by copper/constantin thermocouples and platinum resistance thermometers. The outputs from the platinum resistance thermometers were used to trigger electro-mechanical switches and valves to control the temperature cycle.

Temperature cycles were applied to the specimen by heating and cooling the top and bottom flanges of the specimen (representing external surfaces of the structure) more rapidly than the webs (representing internal structure) to produce a temperature lag between the two and induce thermal stress. This was achieved by heating the flanges first to the required maximum temperature. Before the maximum temperature was reached the heaters were switched off and the residual heat in the duct system was sufficient to bring the specimen up to the required temperature. The temperature of the flanges was then maintained to within $\pm 1\frac{1}{2}^{o}C$ by using a constant source of heat and switching a smaller source of heat. In tests representing service conditions the flanges were kept at maximum temperature for about 90 minutes while the webs were allowed to heat up naturally and in tests representing Concorde Major Fatigue Test conditions the maximum flange temperature was maintained for about 20 minutes while heat was applied to the webs to bring them to the temperature appropriate to the end of the cruise phase. Then all heating was switched off and the flaps in the flange duct circuit were operated to allow ambient air to be blown over the flange surfaces to cool them. In the web duct circuit, the centrifugal fan was stopped so that the webs would cool comparatively slowly by conduction to the flanges. When ambient air could no longer sustain the required rate of cooling of the flanges, liquid nitrogen was introduced into the air-stream in controlled quantities to maintain the rate of cooling until the required minimum temperature of the flanges was achieved. At this point the controllable flaps in the web duct circuit were operated, and ambient air was used to increase the cooling rate of the webs. Coincidentally, in the flange duct circuit, liquid nitrogen injection in the air-stream was stopped and ambient air was used to raise the temperature of the flanges. When all the specimen test section had attained a common temperature, one temperature cycle had been completed.

Throughout the thermal phase of the testing cycle the specimen was protected against incorrect maximum and minimum temperatures and various stages of the thermal cycle were timed and protected by time switches to avoid unrepresentative dwells occurring due to malfunction. To cater for variations in the temperatures of the liquid nitrogen and ambient air, the rate of cooling

was controlled by comparing the readings from the control platinum resistance thermometers at station C of the specimen (see Fig.6) and an electrical voltage ramp. Adequate interlocks between the thermal and mechanical load controllers ensured that both sequences were correctly phased.

Appendix C

LOAD AND TEMPERATURE SEQUENCES USED IN FATIGUE TESTS

The specimens were tested using simple flight-by-flight load and temperature sequences based on those experienced by the Concorde wing structure. Four different sequences were used, two based on aircraft service loadings and two representing the corresponding CMFT loadings. Three specimens were tested under each of the four load and temperature sequences.

The Service temperature sequences were simple representations of the conditions experienced by the aircraft wing during a typical supersonic flight (see Fig.8). The mechanical loading simulated a ground-air-ground cycle and included a period of steady load representing the cruise followed by a number of constant amplitude gust cycles, with load levels adjusted so that the predicted test life of the joint was about 10000 cycles (three years). During the cruise phase of the sequence, thermal stresses were induced in the specimens by first heating and then cooling the flanges relative to the webs thereby representing conditions in deep structure at the beginning and end of supersonic cruise. Two different degrees of thermal stress fatigue damage were investigated and the two Service load and temperature sequences were designed such that an estimated 40% or 80% of the fatigue damage accumulated during each sequence was caused by the thermal stress cycle.

At the start of the Service 80 loading sequence when the flange and web temperatures were about the same, a steady load was applied to represent the cruise condition. To simulate the onset of kinetic heating the flanges were heated rapidly by forced convection while the webs in still air were allowed to heat up slowly by conduction from the flanges. The difference between the web and flange temperatures resulted in the development of thermal stresses - compressive in the flanges and tensile in the webs - which reached a maximum when the flange temperature reached its maximum value. The flange temperature was then maintained for 90 minutes to represent the cruise phase of a supersonic flight, during which time the webs were heated by conduction until they reached their maximum temperature, reducing the temperature differential between the flanges and webs to approximately $10^{\circ}C$. At this stage the thermally induced stresses in the flanges and webs were relatively small. The flanges were then cooled by introducing a cold air flow followed by controlled liquid nitrogen injection, to a temperature lower than the starting point of the cycle while the webs were allowed to cool slowly in still air by the conduction of heat to the flanges. When the flanges reached minimum temperature, the thermal stresses induced were a maximum in the opposite sense to that during the heating phase - tensile in the

flanges and compressive in the webs. At this stage the webs were cooled and the flanges were heated by ambient airflow and mutual conduction until their temperatures returned to the initial values and the thermal stresses decayed. Once the temperatures of the webs and flanges differed by less than approximately $7^{o}C$, the mechanical load sequence was completed by applying seven load cycles to represent gust loading followed by a small reverse mechanical load to represent landing. After the small reverse mechanical load the temperatures of the flanges and webs were approximately $25^{o}C$. The flange was allowed to stay at this temperature while the web was cooled to the temperature specified for the start of the next thermal cycle.

The load and temperature sequence used for the Service 40 case differed in that during the initial heating of the flanges the webs were also heated to reduce the maximum temperature difference between the webs and flanges so that the first thermally induced stress was smaller than in the 80% thermal damage case. A similar technique was adopted during the cooling of the flanges to reduce the second thermally induced stress. In addition, 21 gust cycles were applied in the 40% case to increase the mechanical fatigue damage and maintain the total fatigue damage per flight cycle at the same level as the 80% case.

The CMFT load and temperature sequences (see Fig.9) were designed to be as fatigue damaging as two of the simplified Service load and temperature sequences, i.e. to achieve an acceleration factor of 2 with respect to the Service cases. The mechanical loading was the same as for the Service cycle but it was applied twice during each CMFT cycle. During the first mechanical loading sequence there was a cruise period during which the temperatures of the webs and flanges were varied in the same way as in the Service cases, but over a larger temperature range. This cruise period was of 20 minutes duration rather than 90 minutes as used in the Service case and additional heating was applied to the webs in order that the correct web temperature would be attained at the end of this much shorter cruise period. No cruise phase or thermal cycle was applied during the second mechanical loading sequence of the CMFT cycles. As in the Service cases, the two load and temperature sequences were designed such that either 40% or 80% of the fatigue damage which occurred in each sequence was caused by the thermal stress cycle. This was achieved using the same techniques as used in the Service cases.

Appendix D

TEMPERATURE AND STRESS DISTRIBUTIONS IN THE SPECIMEN

Throughout all tests specimen temperatures were monitored on the thin skins at the centres of the webs and flanges at Station C. For each temperature cycle typical variations of temperature at these positions are shown in Figs.11 to 14. The actual temperatures experienced by the boxes were in good agreement with the nominal values (see Figs.8 and 9). To illustrate how the flange and web temperatures varied along a box during the heating of the flange and at the end of the subsequent cruise period, temperature readings taken during a CMFT 80 cycle are plotted in Fig.15. During the heating phase, flange temperatures at stations upstream of Station C were higher than those downstream where the air was cooler having given up some of its heat to the specimen. At the butt strap joint, however, the additional mass of the joint members caused an appreciable thermal lag (see Fig.15a). During this phase the temperatures at the centre of the web rose slightly but remained fairly uniform along the length of the specimen. By the end of the cruise period the temperature at the centre of the tension flange was quite uniform along the specimen and so was the temperature at the centre of the web. At this stage the web temperature was approximately $10^{\circ}C$ less than that of the flange (Fig.15b).

Figs.16 and 17 indicate the extent to which thermal lag affected the temperature distribution during the CMFT 80 thermal cycle. In addition to showing the thermal lag on the tension flange at the butt strap joint, Fig.16 illustrates how the temperature at the edges of the flanges lagged behind that at the centre. Fig.17 shows how the temperature at the edge of the webs varied faster than that at the centre of the web, both at Station C and at the butt strap joint, i.e. Station D. These effects were the result of conduction between the flanges and webs at the corners of the specimens and meant that the temperatures at the centres of the flanges and webs were closer to the nominal values than the temperatures at the edges. As a result the thermal stresses in the butt strap joint were higher at the centre of the specimen than at the edges.

Combined mechanical and thermal stresses in the tension flange were determined from the readings of strain gauges mounted longitudinally on the skin at the centre of the flange at Station C. These were factored to obtain the average net stress at the butt strap joint. Recorded variations of total net area stress at the joint with time are shown in Figs.18 to 21 for each load and

temperature sequence. (Strain and temperature readings are not available for boxes 21 and 22.) These figures show how the applied mechanical stresses were modified by superimposed thermal stresses. In each case the total stress in the tension flange was reduced to a minimum by the compressive thermal stress which occurred as the flange was heated, and then it was increased to a maximum by the tensile thermal stress which occurred as the flange cooled. In each sequence the gust loading cycles were applied when the temperature difference between flange and web was less than about $7^{o}C$.

Appendix E

ANALYSIS OF FATIGUE CRACKING

During testing the butt strap joint was the only location at which fatigue cracking occurred in all specimens. On some specimens cracks did occur at other locations but these were not extensive and therefore were regarded as incidental.

Two stages of fatigue damage were most readily identified in each specimen, the first crack and final failure. The first crack was defined as the earliest crack detected by radiographic examination and was about 0.1in long (see section 4) and at final failure fatigue cracking was so widespread that most of the load was carried in the boom angles at the joints between the tension flange and shear webs. On the radiographs it was sometimes difficult to distinguish between cracks in the paint and interfay compound at the joint and fatigue cracks in the metal. In addition the accuracy with which the number of cycles to first crack could be measured was limited by the frequency of radiographic examinations, which were carried out at approximately 200 cycle intervals in both the Service and CMFT tests.

Crack growth at the butt strap joint during each test is shown diagrammatically in Figs.22 to 33. First crack and failure always occurred at the most heavily loaded sections, i.e. damage in the butt strap and stringers occurred at either rivet row C or rivet row D and damage in the skin and stringers occurred at either rivet row A or rivet row F. It is seen that the first crack and failure did not always occur at the same location and in some cases large cracks occurred at more than one rivet row. The Figures also show that there was a tendency for crack growth at the butt strap joint to be most rapid from cracks which initiated between the stringers near the longitudinal centreline of the tension flange. This is explained by the higher thermal stresses which occurred at the centres of the flanges (see Appendix D).

Some sections of the crack surfaces from specimens tested under each load and temperature sequence were examined using a scanning electron microscope and they were all found to be similar. The fracture surfaces showed characteristics typical of fatigue failure and striations were clearly visible (see Fig.34). There appeared to be only one striation per complete load and temperature sequence, in each case. Wider examination of the fracture surfaces showed that striations were very closely spaced near the edge of rivet holes (i.e. that part of the fracture surface showing early crack growth) and became more widely spaced away from the rivet holes as cracks propagated. It was not possible to compare crack rates from striation spacings owing to difficulties in finding exactly comparable cracking conditions in different specimens.

Appendix F

STATISTICAL APPRAISAL OF RESULTS

The numbers of cycles to first crack and failure given in Table 1 were used to assess the scatter in the test results. A log normal distribution was assumed for each group of test results and log mean lives to first crack and failure were evaluated (see Table 1). Although the test results for Box 13 are given they were not used in this analysis as the specimen was considered unrepresentative (see section 5). The estimated variance of each group of results was found to range from 0.00037 to 0.00422 for log lives to first crack and from 0.00061 to 0.00731 for log lives to failure (Table 2).

The estimated variances of the various groups of results were compared using the 'F' test and no significant differences were found at the 10% level[4]. In the light of this result it was assumed that the individual sets of results had a common variance. The best estimate of this assumed common variance was obtained by pooling the individual sample estimates from the separate test conditions using the formula:

$$\text{Common Variance} = \left\{ \frac{\Sigma(x_A - \bar{x}_A)^2 + \Sigma(x_B - \bar{x}_B)^2 + \Sigma(x_C - \bar{x}_C)^2 + \Sigma(x_D - \bar{x}_D)^2}{(n_A - 1) + (n_B - 1) + (n_C - 1) + (n_D - 1)} \right\}$$

where x is log number of cycles

$\bar{x}$ is log mean number of cycles

n is number of tests

suffices A, B, C and D refer to test conditions.

The variances calculated in this way were 0.00191 and 0.00288 for log lives to first crack and failure respectively. These values are compatible with the variance observed in constant amplitude fatigue tests of riveted aluminium alloy structure of about 10^4 cycles duration.

Appendix G

PREDICTION OF SPECIMEN FATIGUE LIVES AND ACCELERATION FACTORS

The predictions of the fatigue lives of specimens under the four load and temperature sequences were based on the stress levels measured during testing (Figs.18 to 21). The stresses measured on specimens subjected to nominally the same loading were averaged and a mean stress sequence was obtained for each condition.

Two methods of stress sequence analysis were used in the fatigue life predictions. These were the Separate Cycle Method[5] and the Range Mean Pair Method. In the Separate Cycle Method the stress sequence was divided into its component cycles, i.e. ground-air-ground cycle, thermal stress cycle and gust cycles and this is illustrated in Fig.35. Fig.35a shows the idealised stress sequence associated withe CMFT 80 test condition and obtained from Fig.20. Fig.35b indicates how this sequence was divided into its component cycles using the Separate Cycle Method. For comparison Fig.35c shows how the same sequence was analysed using the Range Mean Pair Method. In this method the complete stress sequence was studied and the stress cycle with the smallest range was identified. This cycle was then extracted and the remainder of the stress sequence was analysed and again the cycle with the smallest range was identified and extracted. This procedure was repeated until the complete sequence had been divided into its component cycles.

The stress sequences associated with the other test conditions were analysed using the same methods. For both methods of analysis the fatigue damage associated with each component cycle was obtained from S-N data. These data were for light alloy aircraft joints and were from two sources, the BAC Design Data Sheets[3] (Fig.36) and the BAC Standard Curve Equation[5] which is given below

$$N = C\left\{\tfrac{1}{2}\left(x + \sqrt{x^2 + 3mx}\right)\right\}^{-5}$$

where N is endurance in cycles

x is alternating stress

m is mean stress

C is a constant

($C = 9.348 \times 10^9$ when x and m are in hectobars

$C = 6.0 \times 10^{10}$ when x and m are in ksi).

Mechanical and thermal stresses were regarded as equally damaging and no allowance was made for the possible effects of elevated temperature on fatigue behaviour. The fatigue life was calculated using Miner's rule.

Each method of stress sequence analysis was used in conjunction with each set of S-N data and hence four predictions of the fatigue life were obtained for specimens tested under each load and temperature sequence. Acceleration factors were calculated by comparing predicted fatigue lives of specimens tested under Service loadings with those of specimens tested under CMFT loadings. The results are summarised in Table 3. In all four cases the minimum of the thermal stress cycle was below or very close to the minimum stress of the ground-air-ground cycle and therefore both methods of analysis gave essentially the same component cycles and hence the same values of acceleration factor.

In the Separate Cycle Method of analysis the complete stress sequence was divided into component cycles, each of which was associated with a separate loading action. Therefore with this method it was possible to calculate the proportion of the total fatigue damage which was caused by the thermal stress cycle for each load and temperature sequence and these values are also given in Table 3.

Appendix H

TEST ACCELERATION FACTORS

Three specimens were tested under each load and temperature sequence and the results of each group of tests were assumed to have a log normal distribution. Accordingly acceleration factors were calculated using log mean lives to first crack and failure.

Acceleration factors were calculated from the test results in the four ways described below.

Method A

Each box was regarded as an entity for which only lives to first crack and failure were known and no account was taken of damage location. The acceleration factors calculated using this method are given in Table 1.

Method B

When first crack and failure did not occur at the same rivet row, the crack propagation life at the location of failure was added to the life to first crack in order to obtain an estimate of the fatigue life of the specimen if the first crack had propagated, i.e. when first crack occurred in rivet row F, say, in the butt strap joint after N_1 cycles and failure occurred in rivet row C after N_F cycles, if the earliest crack in row C occurred after N_2 cycles, then the modified life to failure, N_{Fmod}, was given by

$$N_{Fmod} = N_1 + (N_F - N_2)$$

N_1 and N_{Fmod} were then used in the calculation of acceleration factors (see Table 4).

Method C

In this method the earliest crack at the location of failure was taken to be the first crack and so, with the notation of Method B, N_2 and N_F were used in the evaluation of acceleration factors (see Table 4).

Method D

The test results were grouped by damage location and acceleration factors were calculated accordingly, i.e. within a group of tests carried out at a particular condition results for specimens with cracks in the skin and stringers

at rivet row A or F were considered together and those with butt strap and stringer cracks at row C or D were analysed together (see Table 5). The significance of the results obtained using this method is questionable as often only one result is available per condition.

Table 1

SUMMARY OF TEST RESULTS

Test condition	Box No.	Number of cycles to first crack, N_1	First crack location (Rivet row)	Number of cycles to failure N_F	Location of failure (Rivet row)	Acceleration factors using Method A: Log mean N_1	Log mean N_F	First crack acceleration factor	Failure acceleration factor
CMFT 80	13	5716	A_a	7500	C_b, C_c				
	20	2894	F_c	4355	F_a, F_c	3220	4640	2.7	3.1
	22	3575	C_b, A_c, A_a	4942	C_b, C_c				
Service 80	14	8889	F_a, C_b	13216	F_a, F_c	8710	14470		
	15	9808	A_c	18142	C_b, C_c				
	16	7576	F_a, A_a	12643	F_a, F_c				
CMFT 40	21	3005	F_c, F_a	6081	F_a, F_c	3110	6450	2.2	2.5
	23	2958	F_c	6205	F_a, F_c				
	24	3381	A_c	7121	C_b, C_c				
Service 40	17	6606	F_a	15974	D_b, D_c	6850	16250		
	18	7194	A_a	17324	F_a, F_c				
	19	6762	C_b	15520	F_a, F_c				

Suffix a = skin, b = butt strap, s = stringer

Table 2

SCATTER IN TEST RESULTS

Test condition	Box No.	Number of cycles to first crack N_1	Log mean N_1	Variance, $V_1 = \frac{\Sigma(\log N_1 - \text{mean log } N_1)^2}{n-1}$ [n = number of tests per condition]	Number of cycles to failure N_F	Log mean N_F	Variance, $V_F = \frac{\Sigma(\log N_F - \text{mean log } N_F)^2}{n-1}$ [n = number of tests per condition]
CMFT 80	13	5716			7500		
	20	2894	3220	0.00422	4355	4640	0.00152
	22	3575			4942		
Service 80	14	8889	8710	0.00321	13216	14470	0.00731
	15	9808			18142		
	16	7576			12643		
CMFT 40	21	3005	3110	0.00101	6081	6450	0.00139
	23	2958			6205		
	24	3381			7121		
Service 40	17	6606	6850	0.00037	15974	16250	0.00061
	18	7194			17324		
	19	6762			15520		

Table 3

PREDICTED FATIGUE LIVES AND ACCELERATION FACTORS

	Separate Cycle Method		Range Mean Pair Method	
	BAC light alloy aircraft joints data	BAC Standard Curve Equation	BAC light alloy aircraft joints data	BAC Standard Curve Equation
CMFT 80 loading.	7400	5470	7180	5400
% thermal fatigue damage	80	90	-	-
Service 80 loading.	13210	11390	13210	11390
% thermal fatigue damage	83	93	-	-
Acceleration factor	1.8	2.1	1.8	2.1
CMFT 40 loading.	7670	9360	7440	9160
% thermal fatigue damage	45	68	-	-
Service 40 loading.	15150	22140	15170	22030
% thermal fatigue damage	46	63	-	-
Acceleration factor	2.0	2.4	2.0	2.4

Table 4

ACCELERATION FACTORS EVALUATED USING METHODS B AND C OF APPENDIX H

							Acceleration factors using Method B					Acceleration factors using Method C			
Loading	Box No.	Number of cycles to first crack N_1	First crack location (rivet row)	Number of cycles to failure N_F	Failure location (rivet row)	Number of cycles to first crack at failure location N_2	$N_{Fmod} = N_1 + N_F - N_2$	Log mean N_1	Log mean N_{Fmod}	First crack acceleration factor	Failure acceleration factor	Log Mean N_2	Log Mean N_F	First crack acceleration factor	Failure acceleration factor
CMFT 80	13	5716	A	7500	C	6388									
	20	2894	F	4355	F	2894	4355	3220	4640	2.7	2.9	3220	4640	3.0	3.1
	22	3575	C and A	4942	C	3575	4942								
Service 80	14	8889	F and C	13216	F	8889	13216	8710	13330			9750	14470		
	15	9808	A	18142	C	13761	14189								
	16	7576	F and A	12643	F	7576	12643								
CMFT 40	21	3005	F	6081	F	3005	6081	3110	5910	2.2	2.4	3550	6450	2.4	2.5
	23	2958	F	6205	F	2958	6205								
	24	3381	A	7121	C	5021	5481								
Service 40	17	6606	F	15974	D	7323	15257	6850	14430			8490	16250		
	18	7194	A	17324	F	8191	16327								
	19	6762	C	15520	F	10214	12068								

Table 5

ACCELERATION FACTORS EVALUATED USING METHOD D OF APPENDIX H

Damage criterion \ Loading	CMFT 80	Service 80	CMFT 40	Service 40
First crack in rivet row A or F	Box 20 at 2894 Box 22 at 3575 Log mean N_I = 3220	Box 14 at 8889 Box 15 at 9808 Box 16 at 7576 Log mean N_I = 8710	Box 21 at 3005 Box 23 at 2958 Box 24 at 3381 Log mean N_I = 3110	Box 17 at 6606 Box 18 at 7194 Log mean N_I = 6890
	Acceleration factor = 2.7		Acceleration factor = 2.2	
First crack in rivet row C or D	Box 22 at 3575	Box 14 at 8889	No result	Box 19 at 6762
	Acceleration factor = 2.5			

Damage criterion \ Loading	CMFT 80	Service 80	CMFT 40	Service 40
Major damage at rivet row A or F	Box 20 at 4355	Box 14 at 13216 Box 16 at 12643 Log mean N_F = 12930	Box 21 at 6081 Box 23 at 6205 Log mean N_F = 6140	Box 18 at 17324 Box 19 at 15520 Log mean N_F = 16400
	Acceleration factor = 3.0		Acceleration factor = 2.7	
Major damage at rivet row C or D	Box 22 at 4942	Box 15 at 18142	Box 24 at 7121	Box 17 at 15974
	Acceleration factor = 3.7		Acceleration factor = 2.2	

REFERENCES

No.	Author	Title, etc.
1	E.L. Ripley, OBE	Structural tests for the supersonic transport aircraft. RAE Technical Report 70121 (1970)
2	F.E. Kiddle R.J. Kite R.F. Mousley	A study of thermal fatigue acceleration in box beams under mechanical and thermal stress. ARC CP No.1342 (1975)
3	-	Structural design data sheets, 3, 43.3.4 and 43.3.8 BAC Ltd.
4	-	Data sheets on fatigue: No. 68016 'Comparison of samples'. Engineering Sciences Data Unit, Royal Aeronautical Society (1968)
5	G.D. Sellers	Cumulative damage calculations associated with accelerated thermal fatigue tests. BAC Ltd., Reference SST/R51/54/0029 (1972)

Note: *References quoted are not necessarily available.*

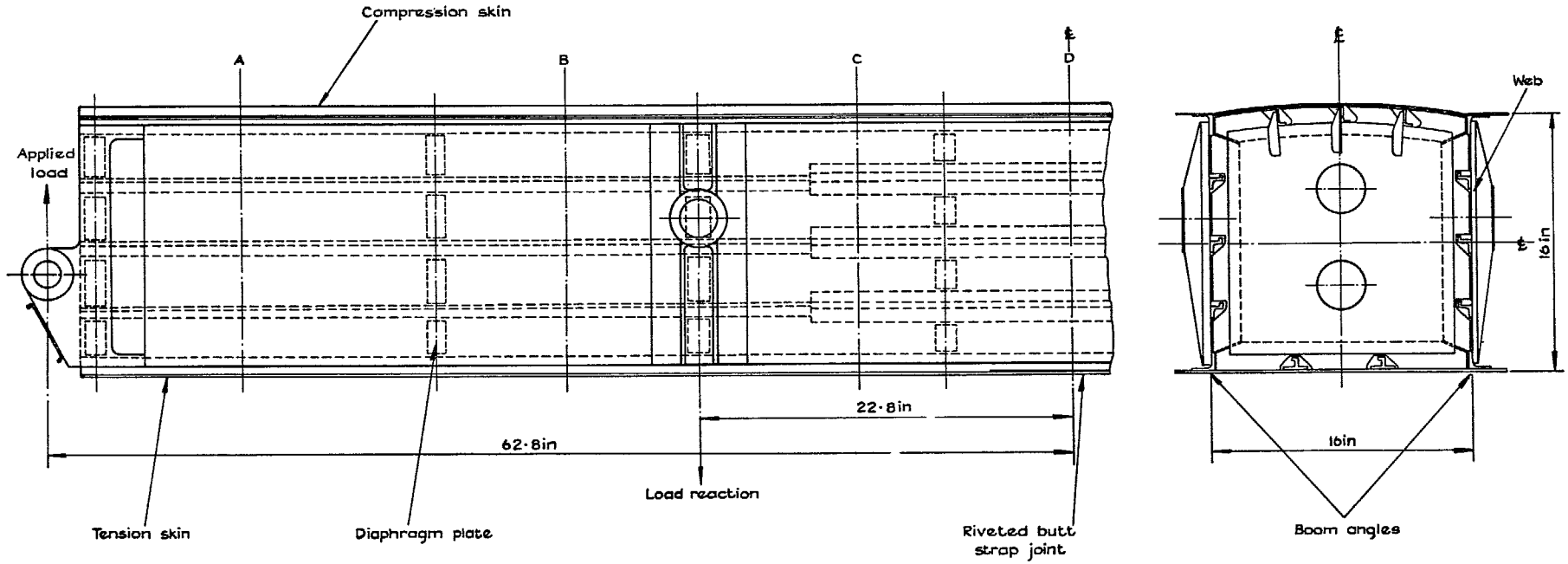

Fig.1 General arrangement of the deep box specimens

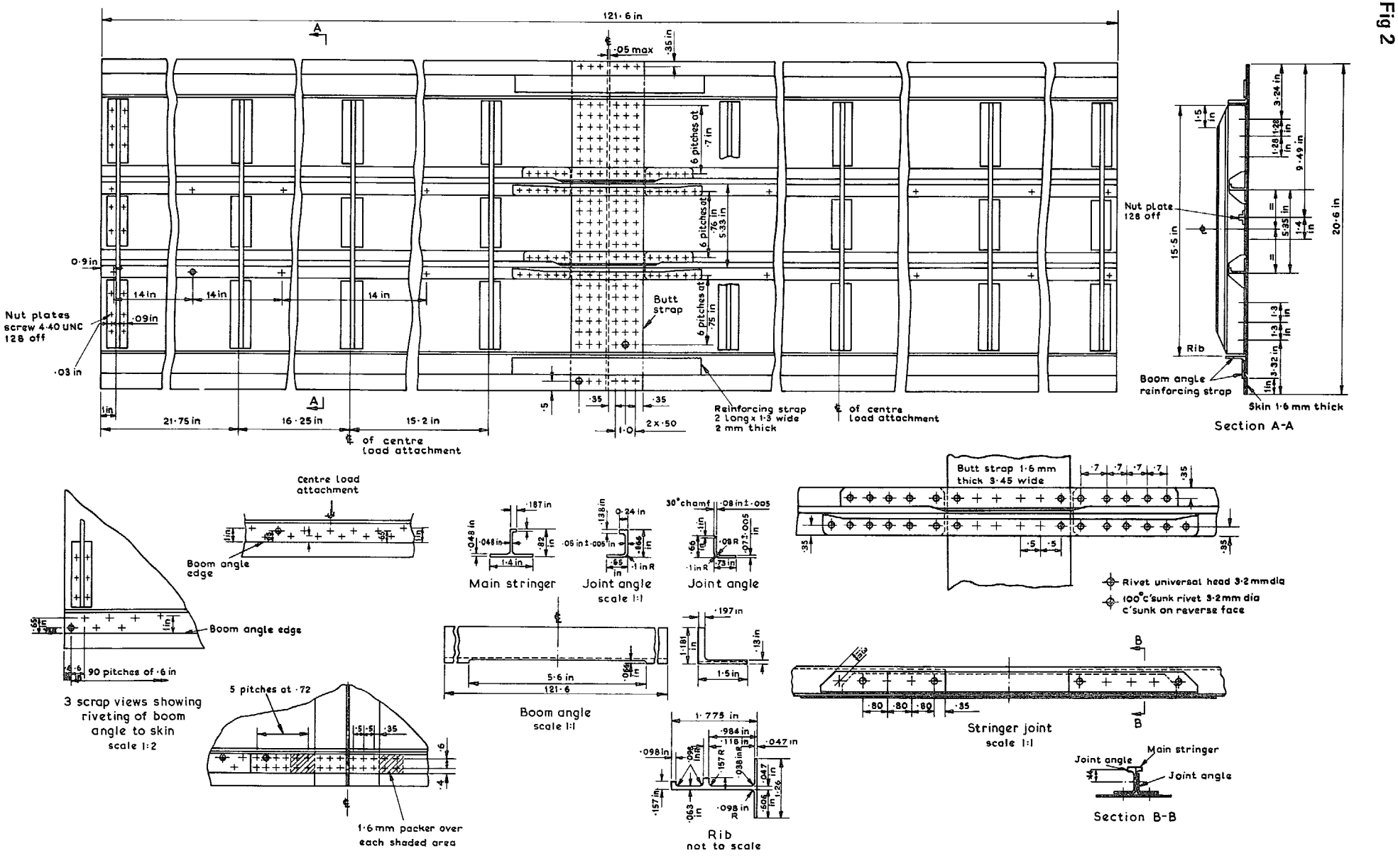

Fig.2 Bottom panel assembly of specimen. Scale 1:2 and 1:1

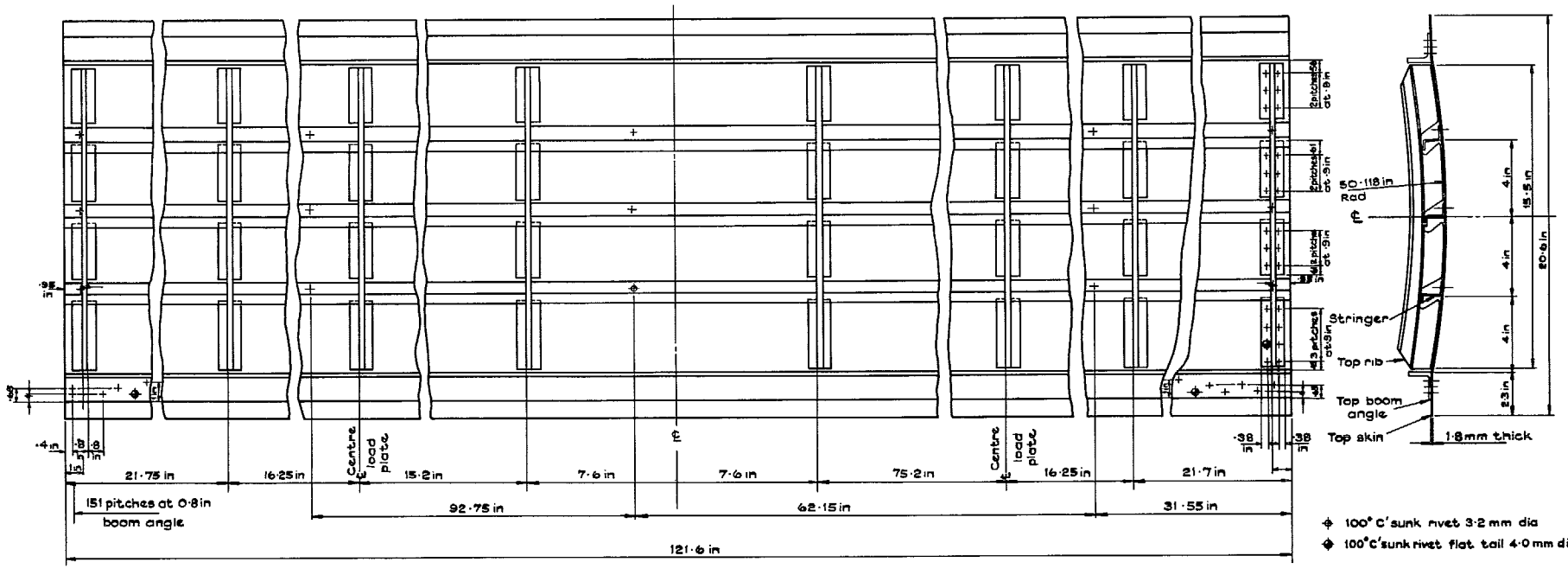

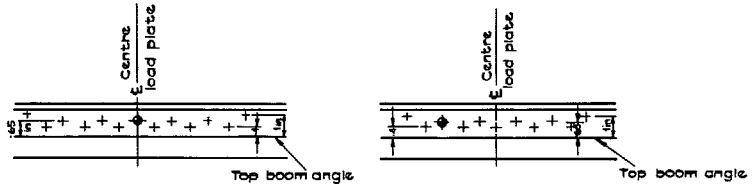

Scrap view showing boom angle rivets vicinity of centre load plates
scale 1:2

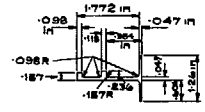

Top rib section
not to scale

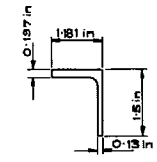

Boom angle section
full size

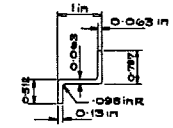

Stringer section
full size

Fig.3 Top panel assembly of specimen. Scale 1:2 and 1:1

Fig 3

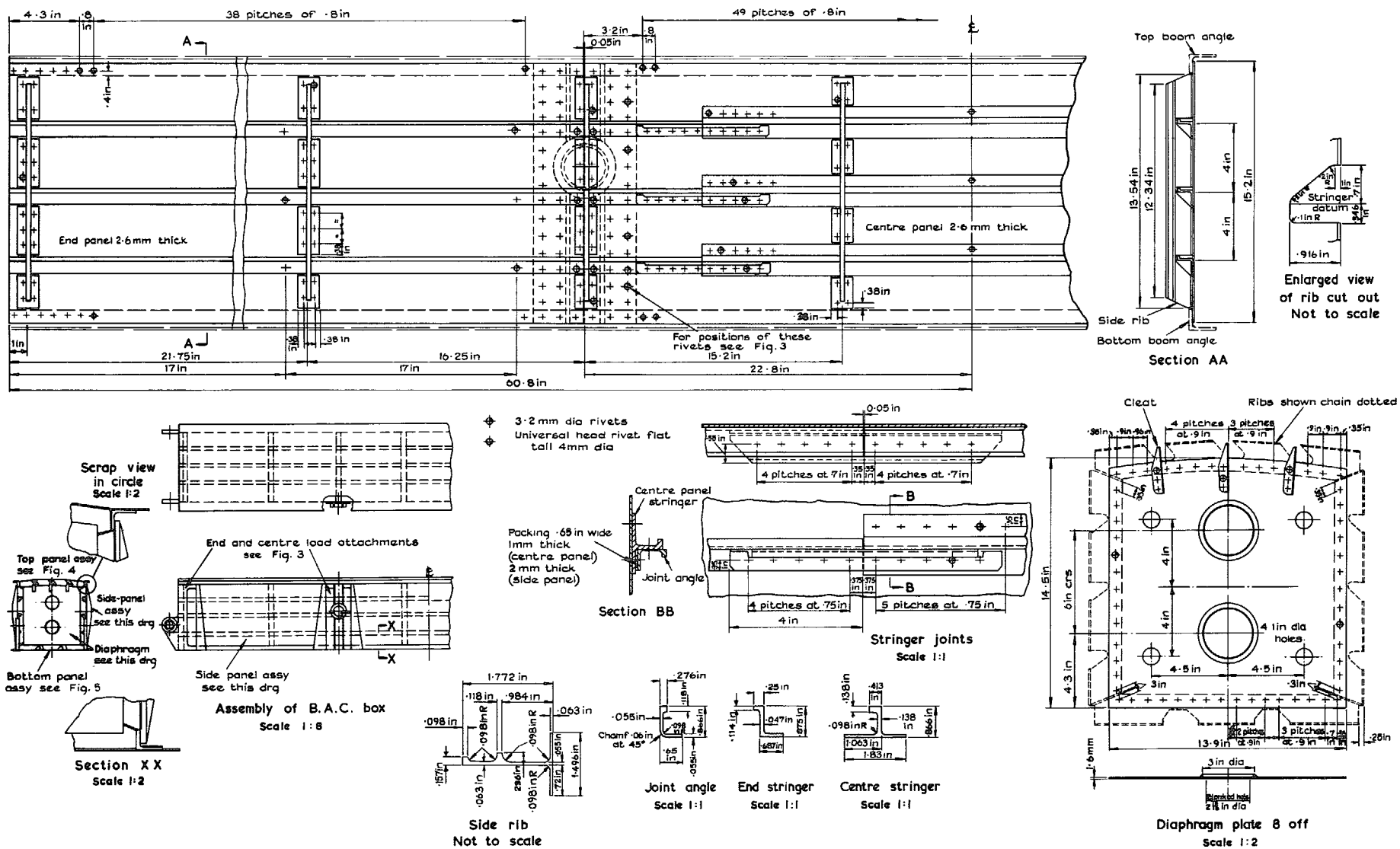

Fig.4 Side panel assembly of specimen. Scale 1:2 and 1:1

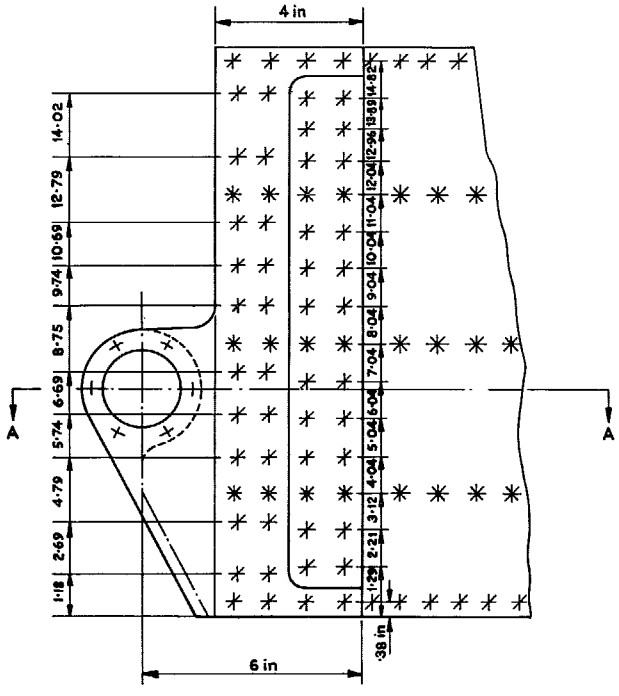

* 4·0 mm rivet univ hd

* 4·0 mm rivet 100° c'sunk hd

* 3·2 mm rivet univ hd

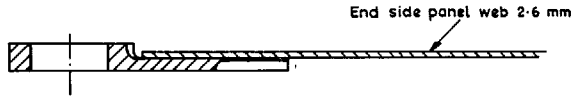

Section AA
End attachment plate

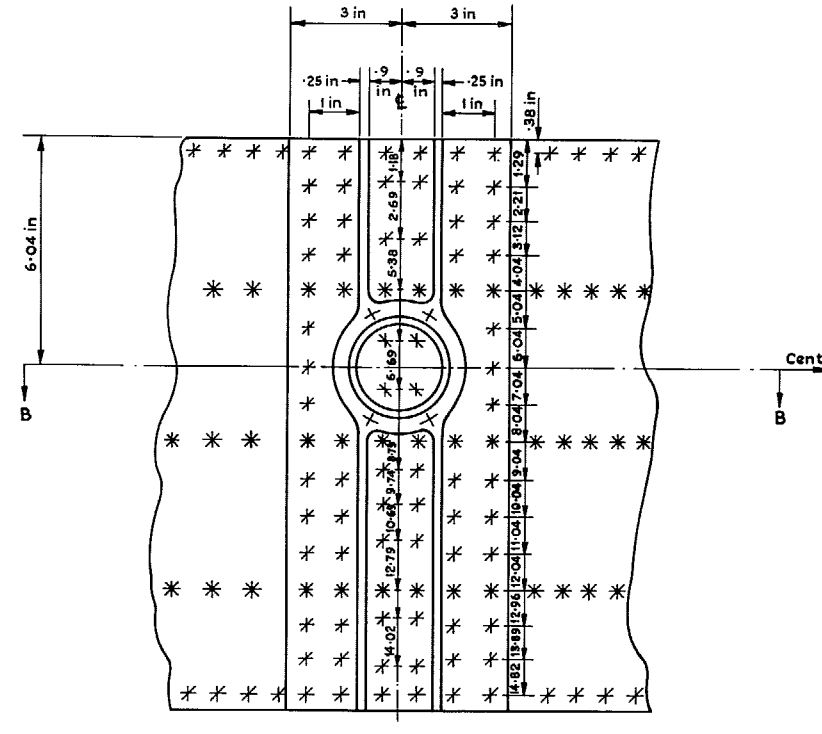

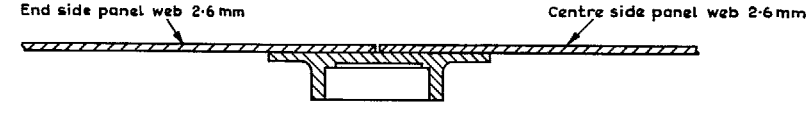

Section BB
Centre load attachment plate

Fig.5 Specimen loading attachments

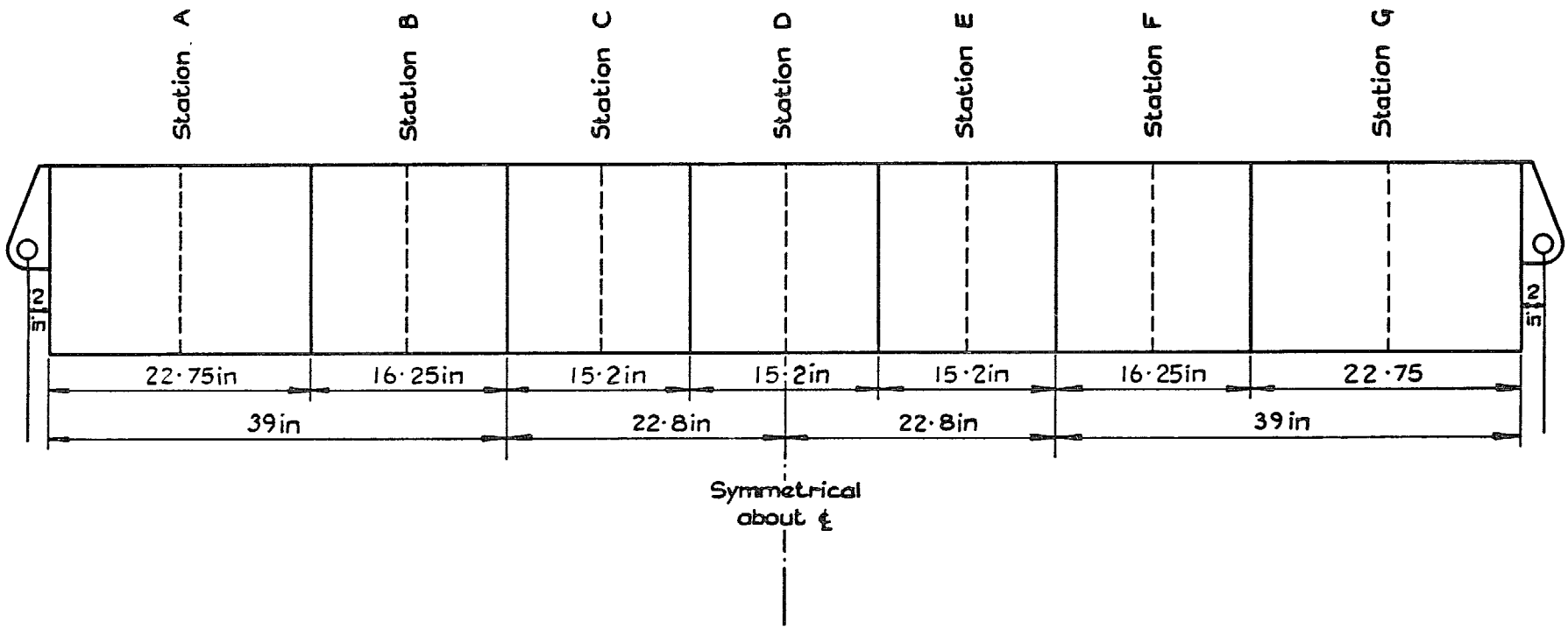

Fig.6 Positions in specimen where strain gauges and thermocouples are attached

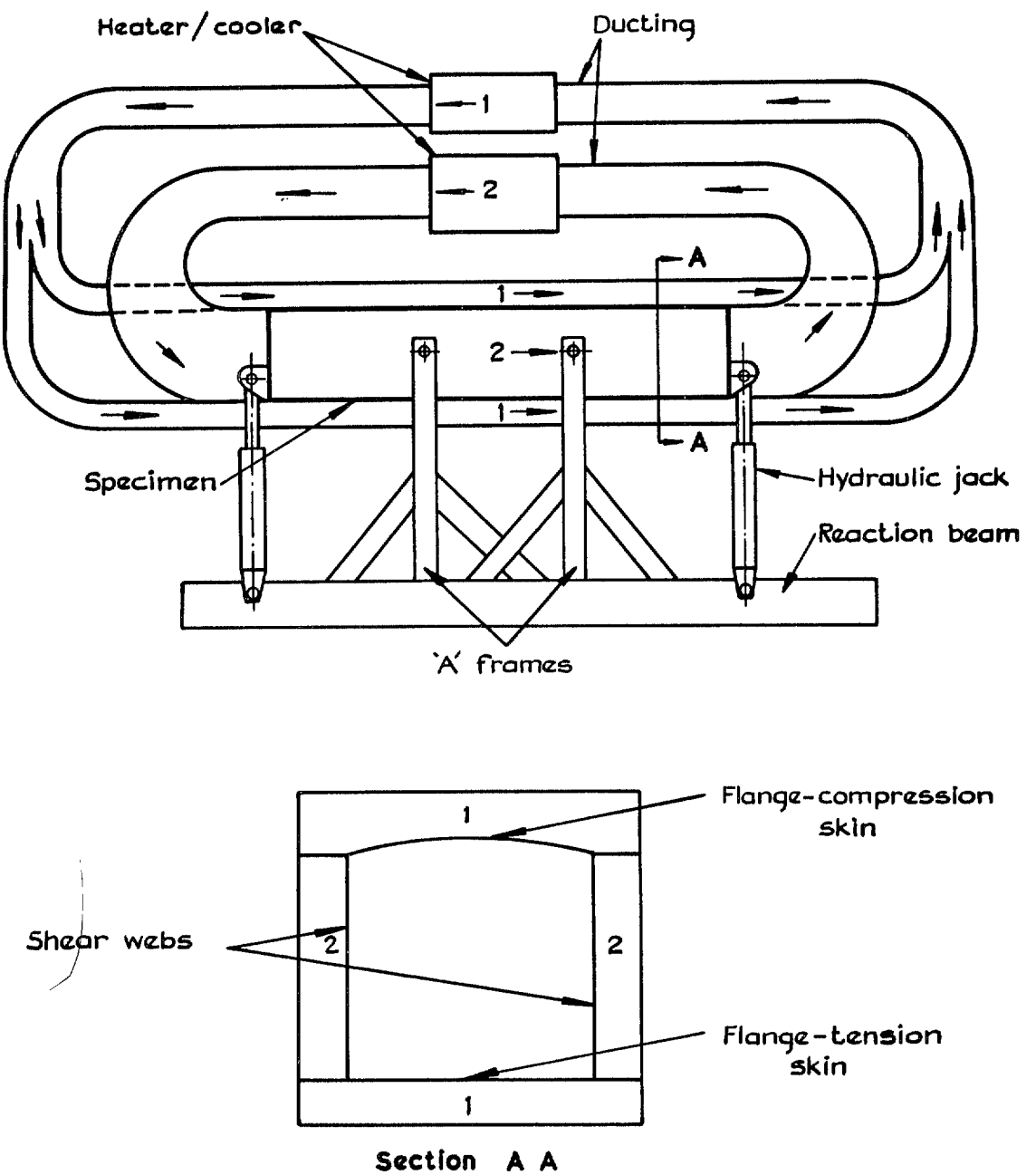

Fig.7 Schematic arrangement of the testing rig

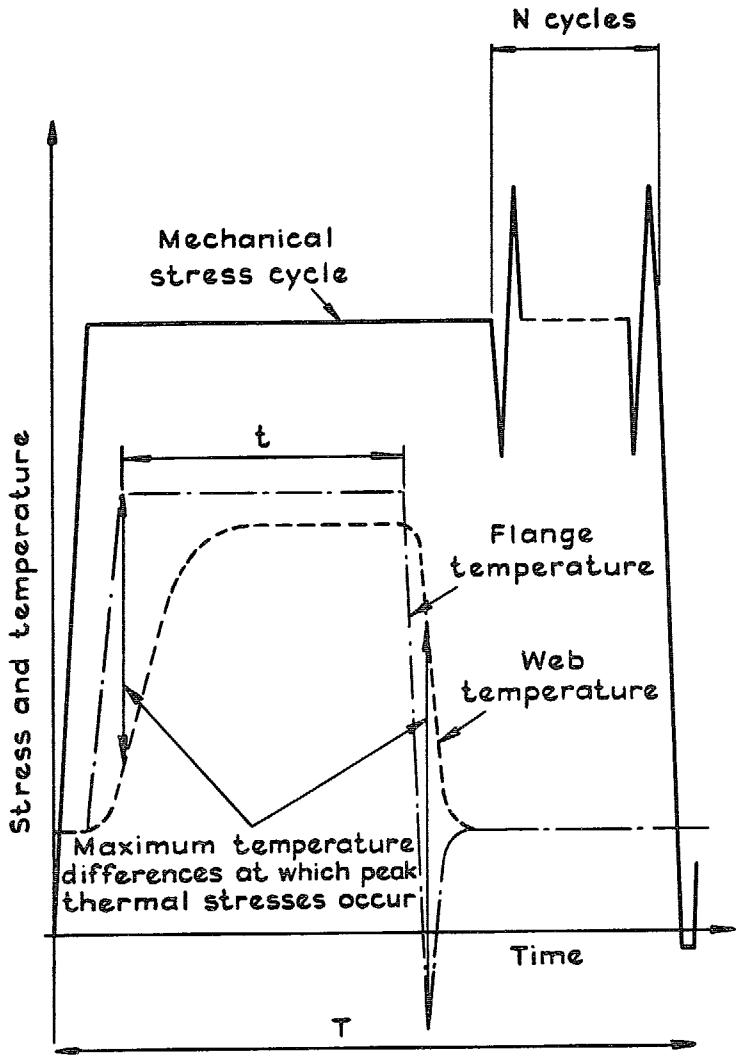

% thermal stress fatigue damage	80		40	
Mean mechanical stress based on nett area at butt strap (ksi)	11·0		11·0	
Nett area gust stress (ksi)	±4·6		±4·6	
No of cycles, N	7		21	
Nominal temperatures at station C (°C)	At centre of flange	At centre of web	At centre of flange	At centre of web
At start of cycle		15		15
At 1st peak thermal stress	100	26	100	43
At end of cruise	100	92	100	92
At 2nd peak thermal stress	-20	75	-20	54
Cruise time t (min)	90		90	
Total cycle time t (min)	~112		~112	

Fig.8 General form of Service load and temperature sequence with table showing nominal values

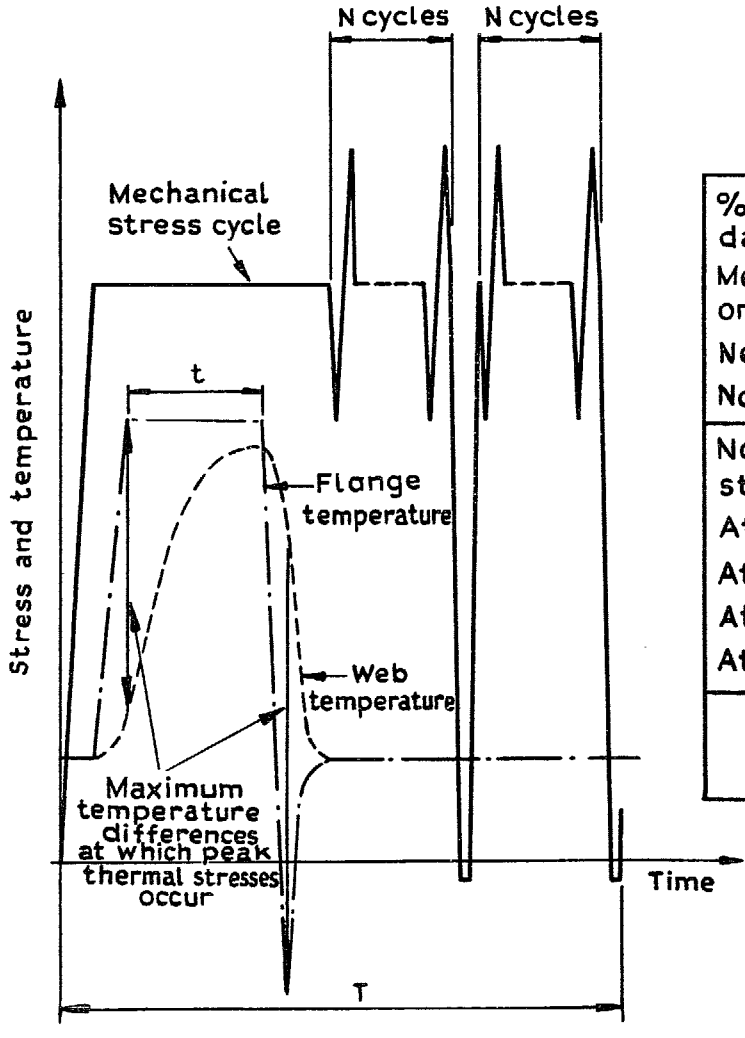

% thermal stress fatigue damage	80		40	
Mean mechanical stress based on nett area at butt strap (ksi)	11·0		11·0	
Nett area gust stress (ksi)	±4·6		±4·6	
No of gust cycles, N	7		21	
Nominal temperatures at station C (°C)	At centre of flange	At centre of web	At centre of flange	At centre of web
At start of cycle		20		20
At 1st peak thermal stress	130	35	130	56
At end of cruise	130	120	130	120
At 2nd peak thermal stress	-25	97	-25	70
Cruise time t (min)	20		20	
Total cycle time T (min)	~43		~43	

Fig.9 General form of CMFT load and temperature sequences with table showing nominal values

Fig 10

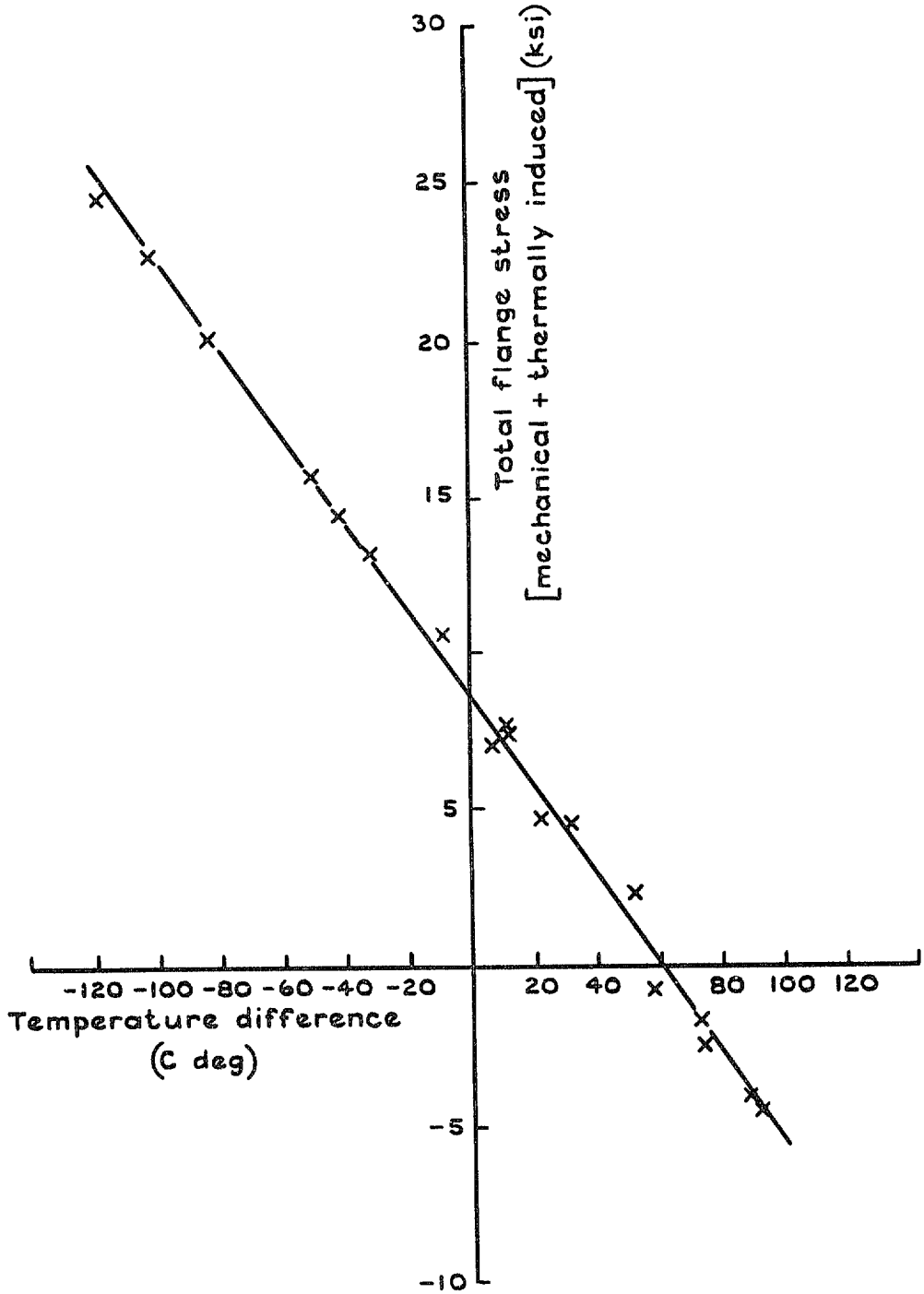

Fig.10 Total flange stress at station C vs temperature difference between webs and flanges at station C

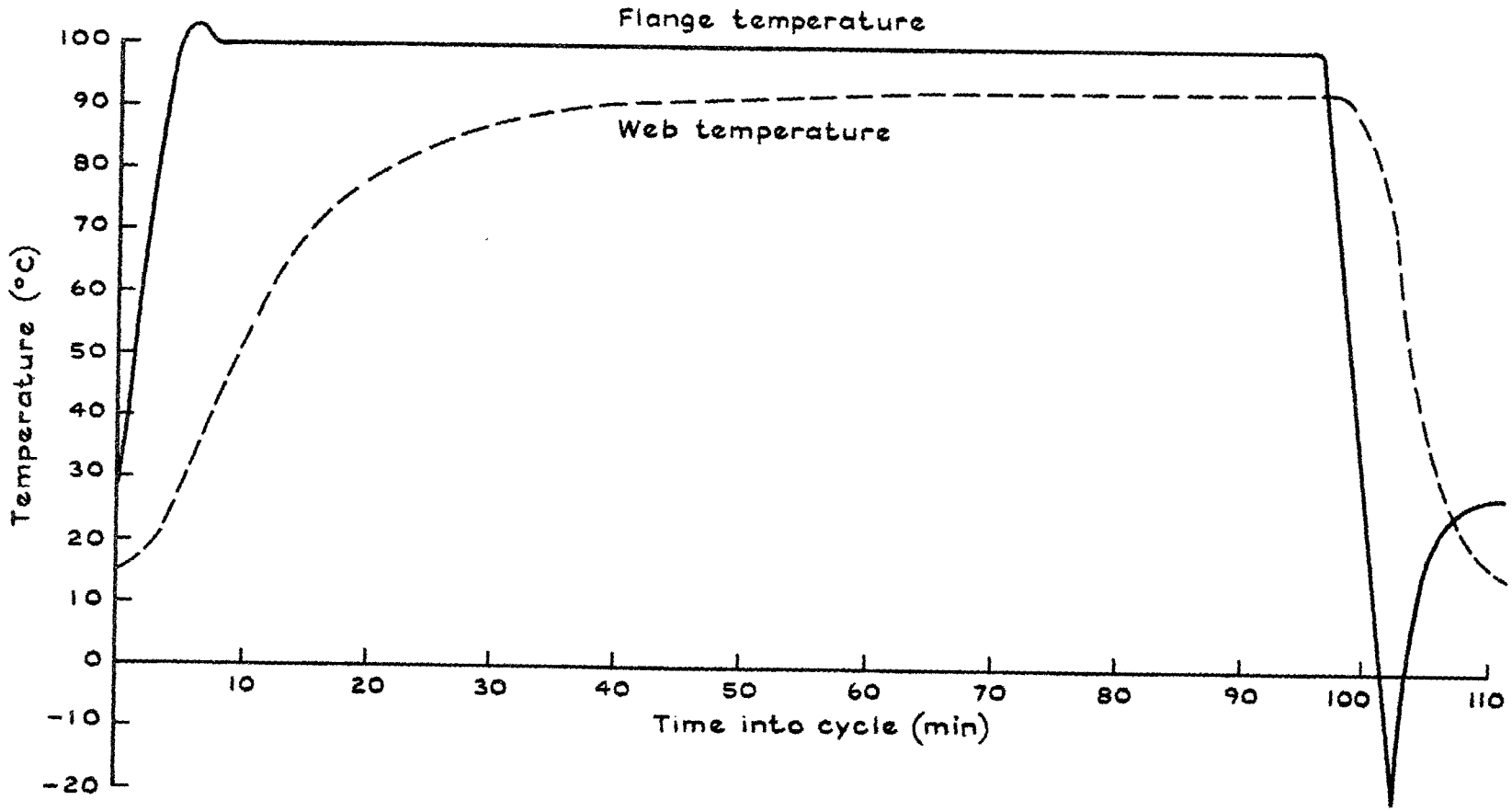

Fig.11 Typical variation of flange and web temperatures at station C during a Service 80 cycle

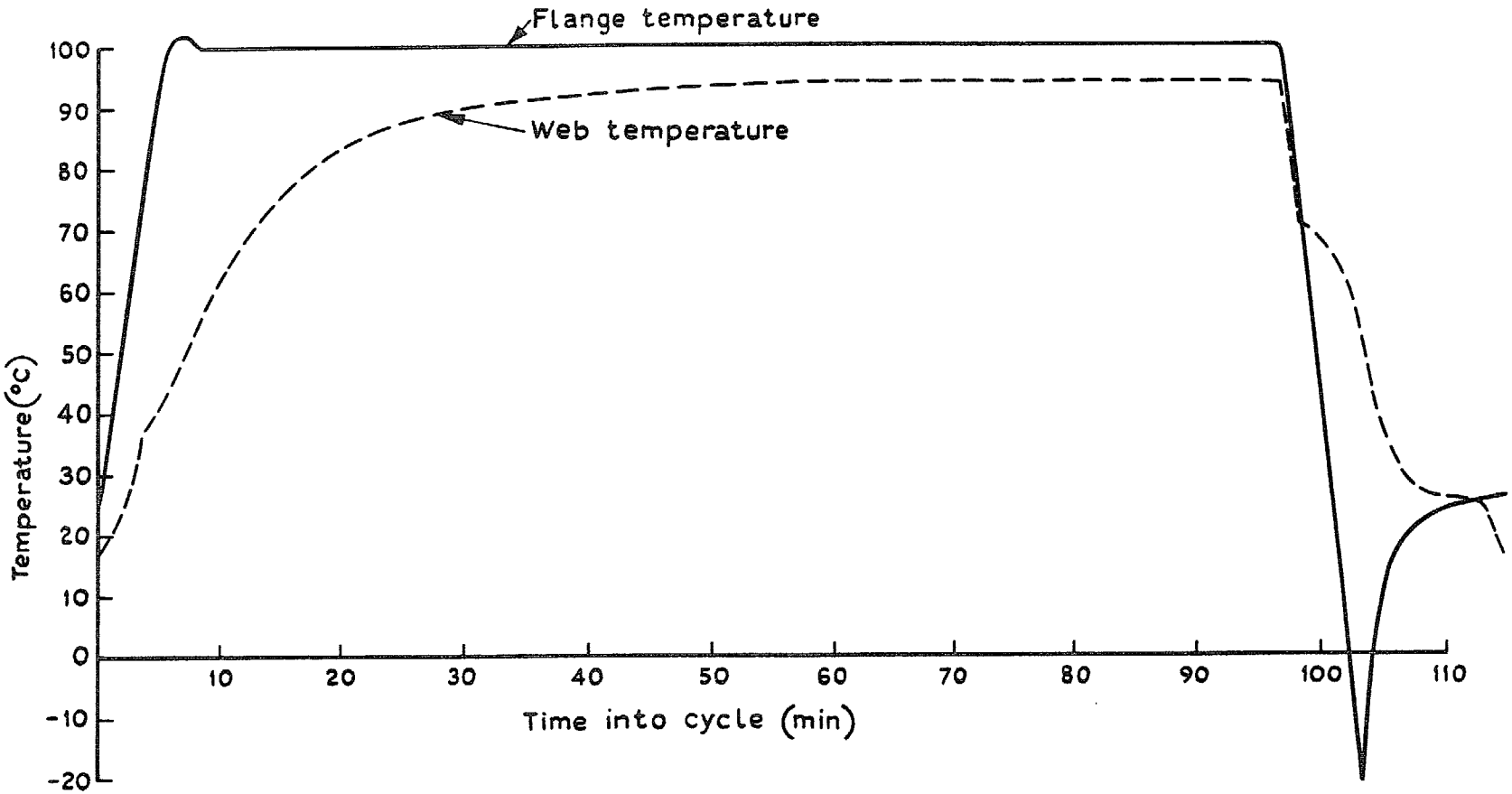

Fig.12 Typical variations of flange and web temperatures at station C during Service 40 cycle

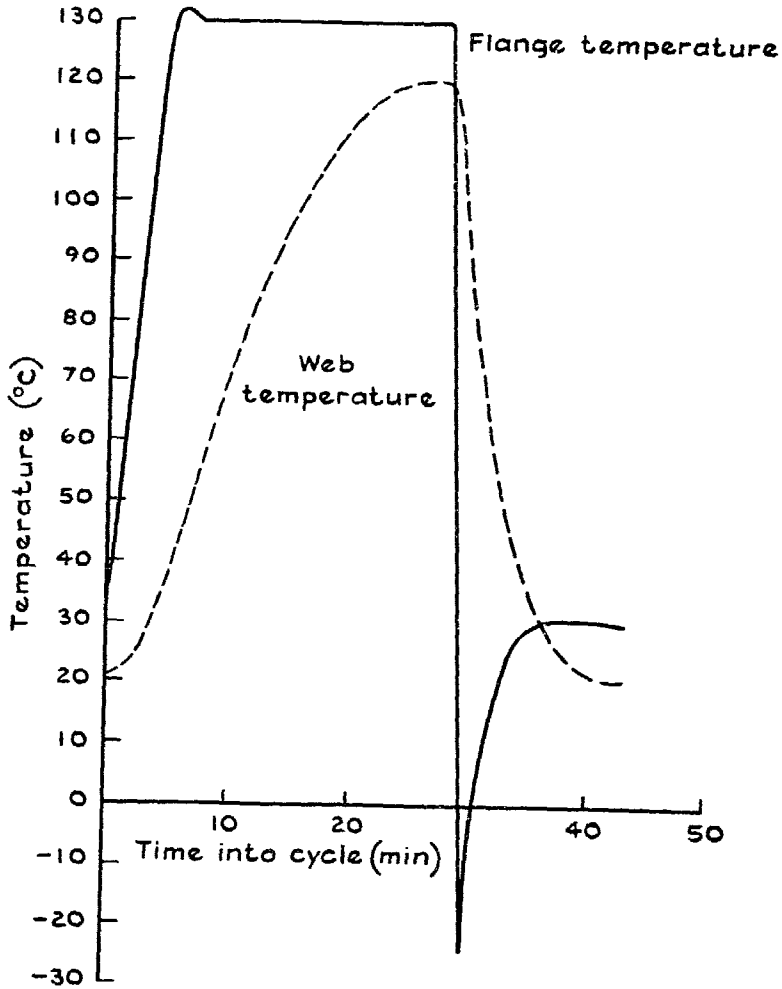

Fig.13 Typical variations of flange and web temperatures at station C during a CMFT 80 cycle

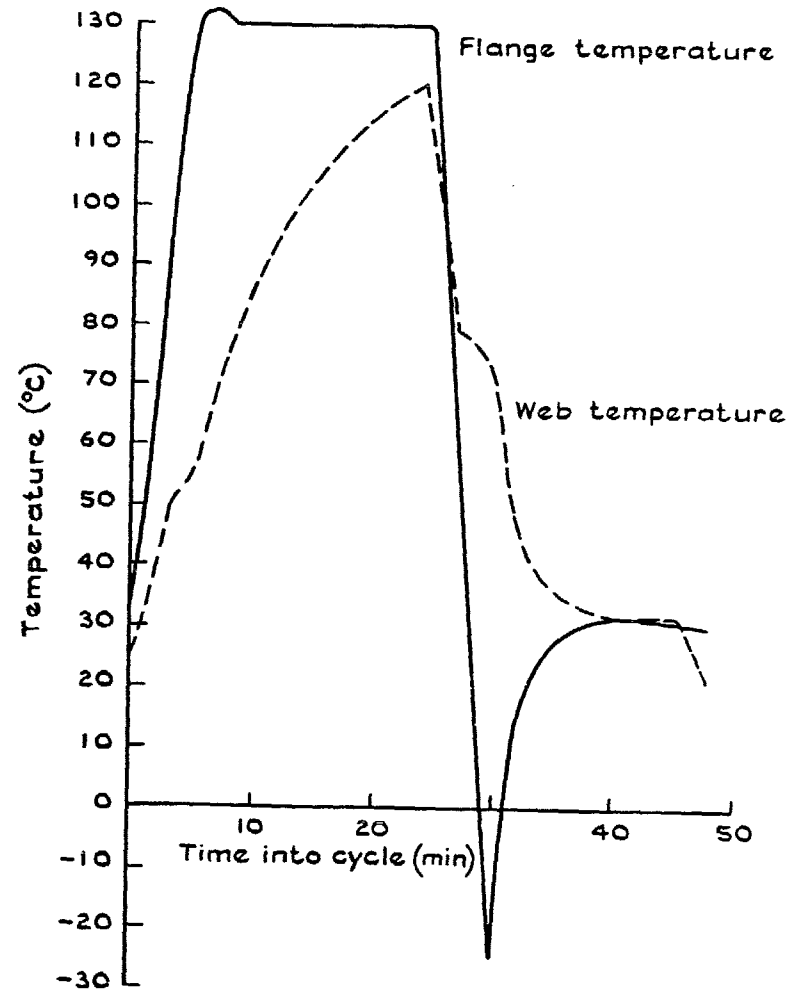

Fig.14 Typical variations of flange and web temperatures at station C during a CMFT 40 cycle

Fig 15a&b

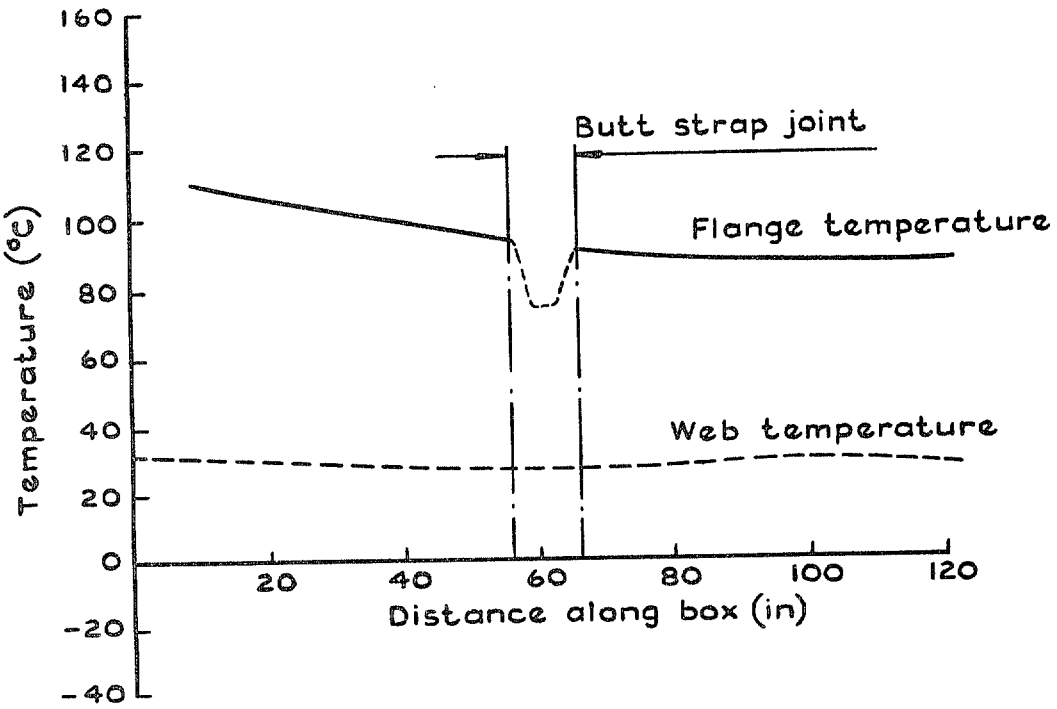

Fig.15a Variation of web and flange temperatures along a box specimen during the initial heating phase of a CMFT 80 cycle

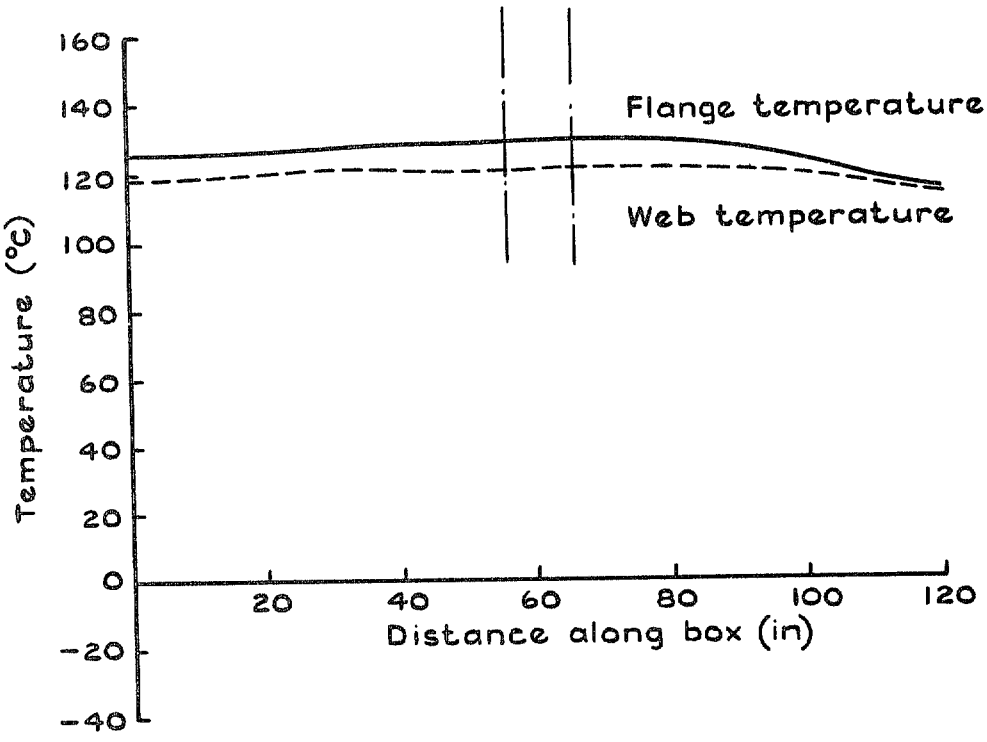

Fig.15b Variation of web and flange temperatures along a box specimen at the end of the cruise phase of a CMFT 80 cycle

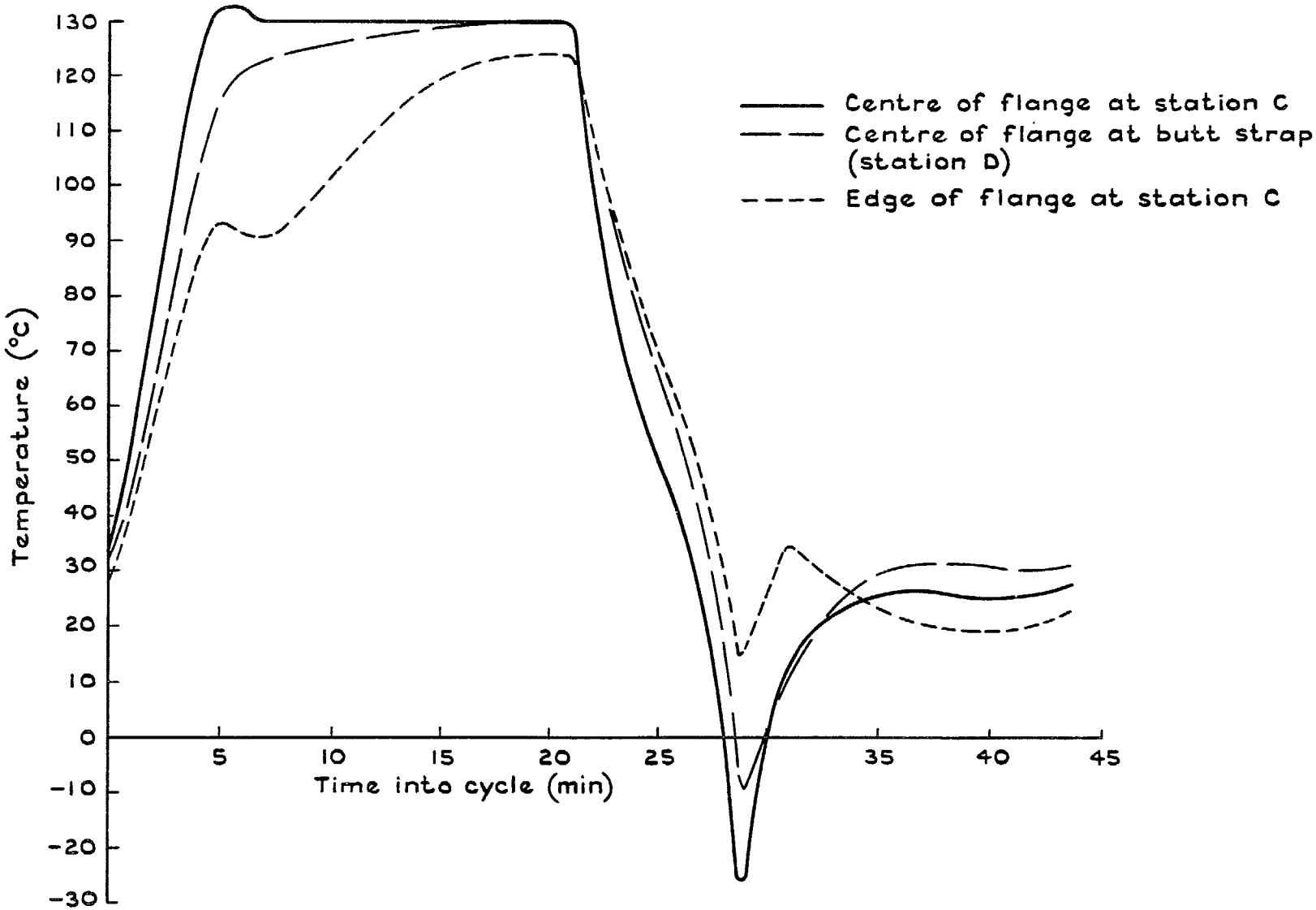

Fig.16 Temperature variation on flange during a CMFT 80 cycle

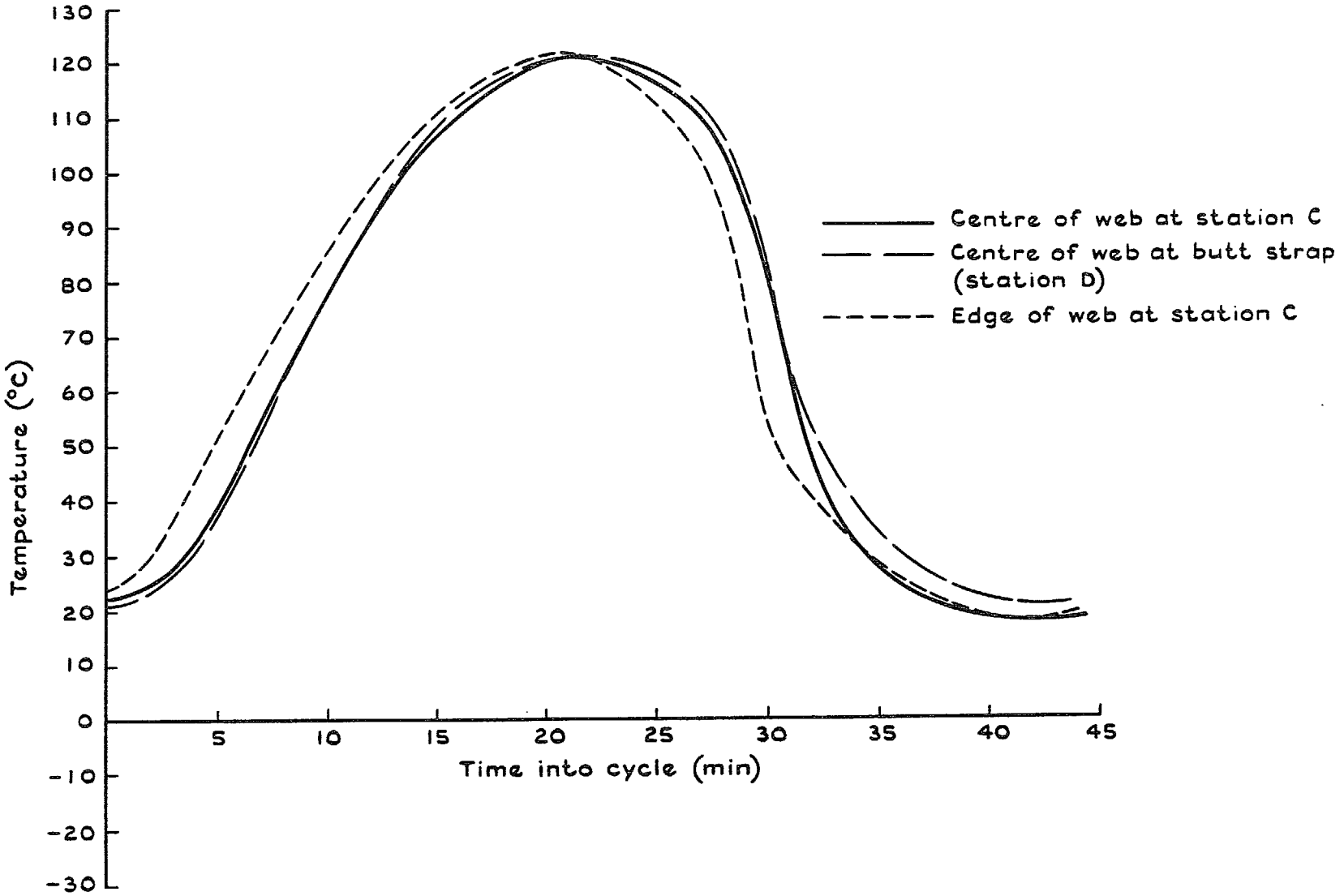

Fig.17 Temperature variation in web during a CMFT 80 cycle

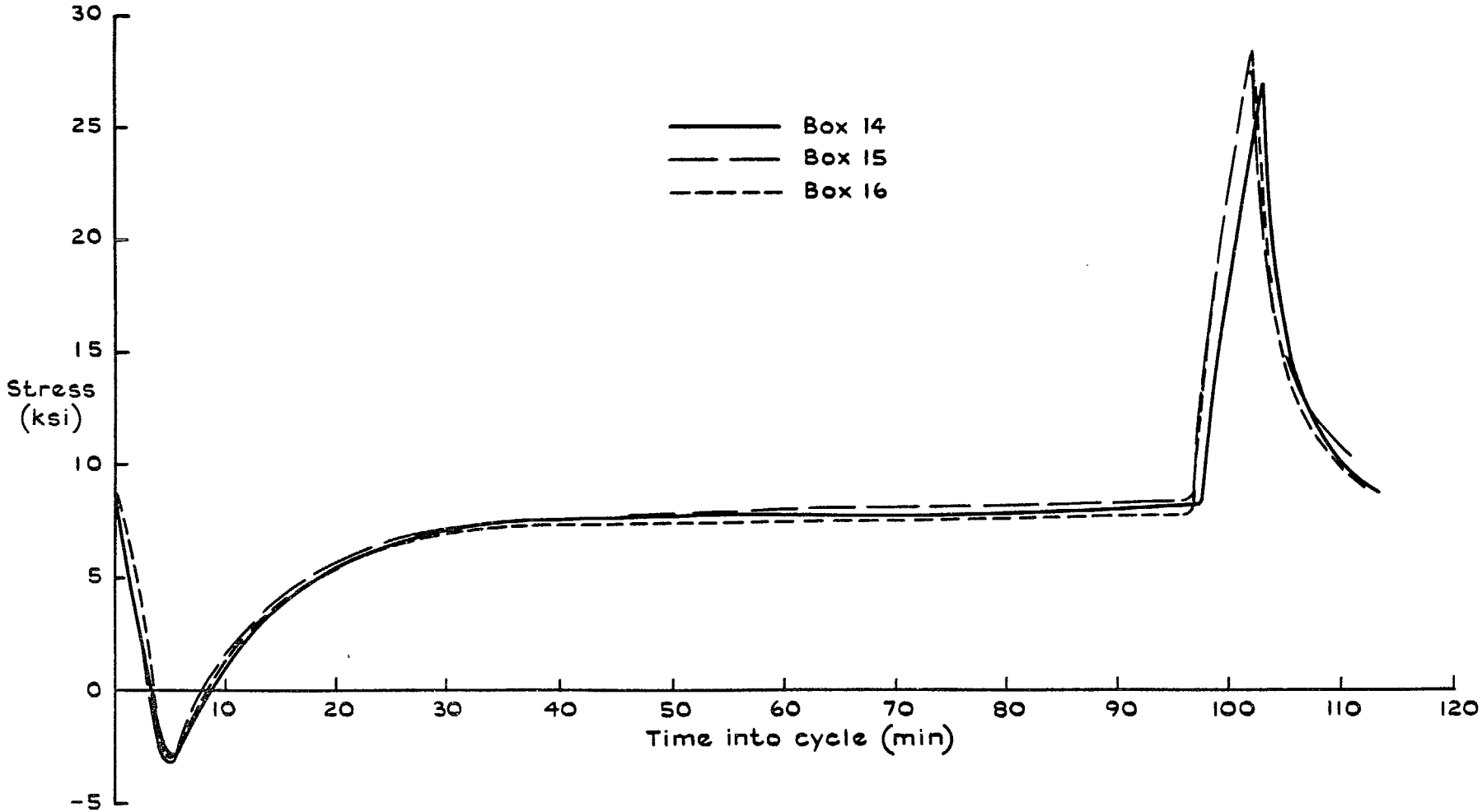

Fig.18 Variation of average net area stress at the butt strap joint with time for specimens tested under the Service 80 load and temperature sequence

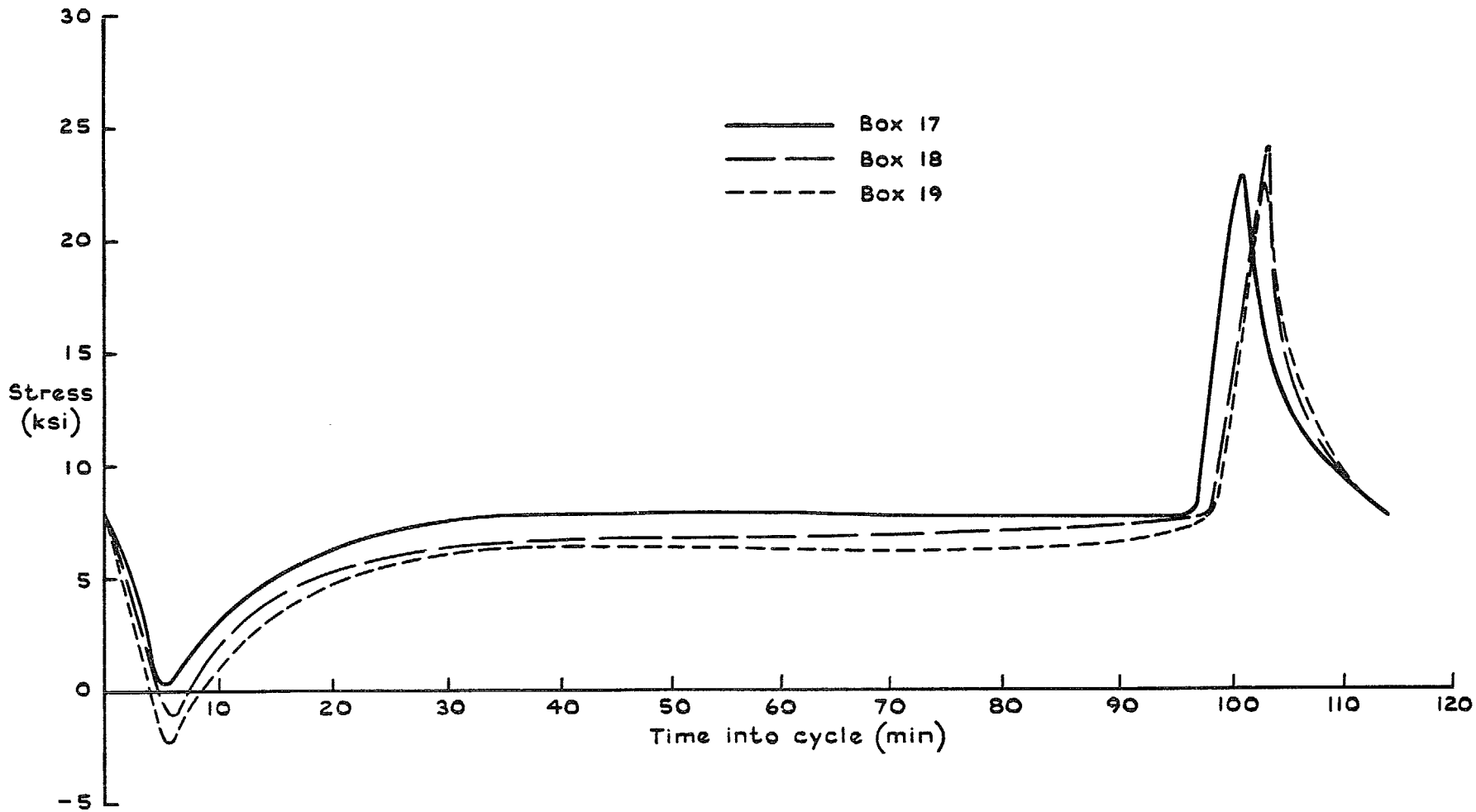

Fig.19 Variation of average net area stress at the butt strap joint with time for specimens tested under the Service 40 load and temperature sequence

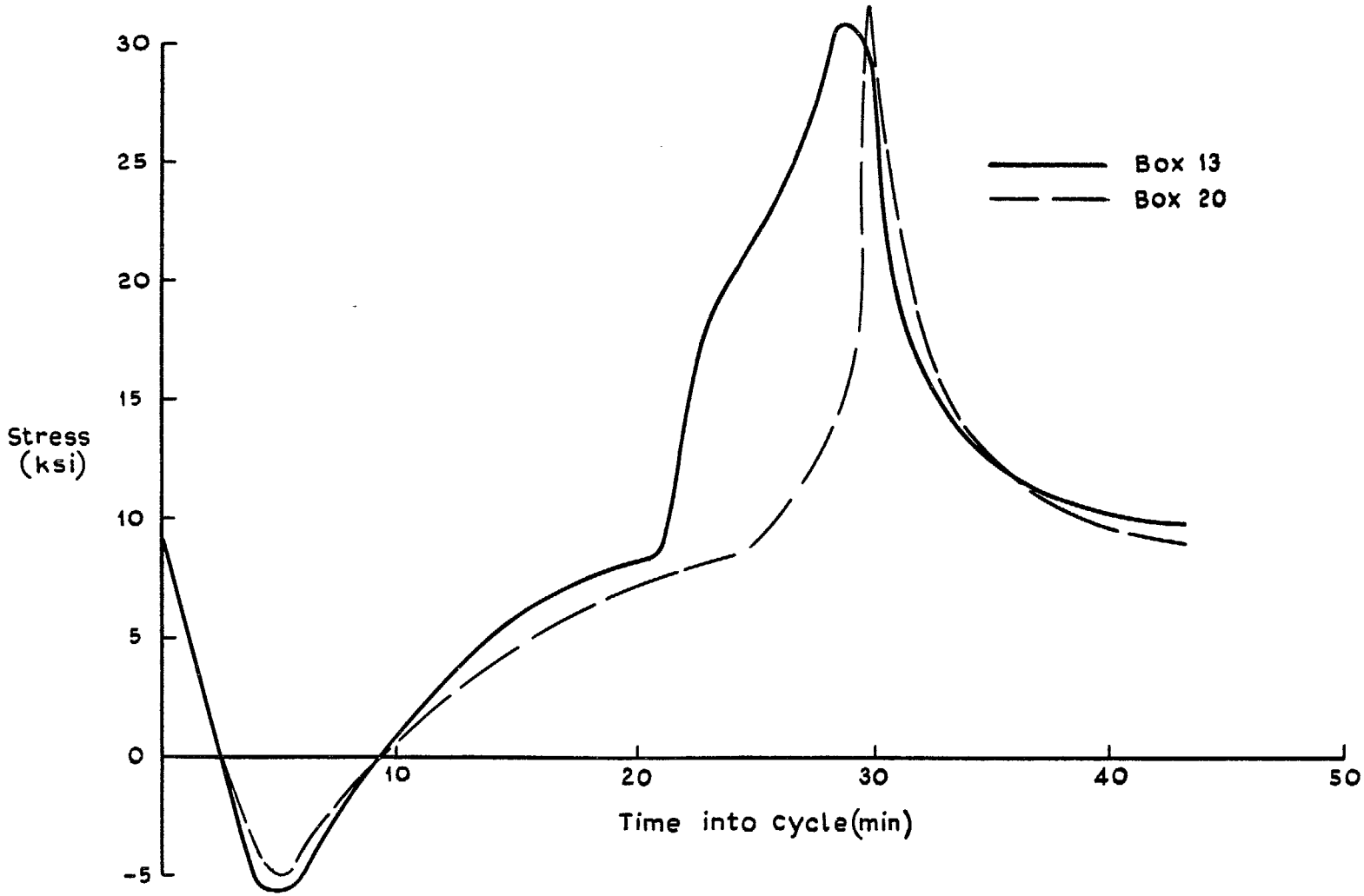

Fig.20 Variation of average net area stress at the butt strap joint with time for specimens tested under the CMFT 80 load and temperature sequence

Fig 20

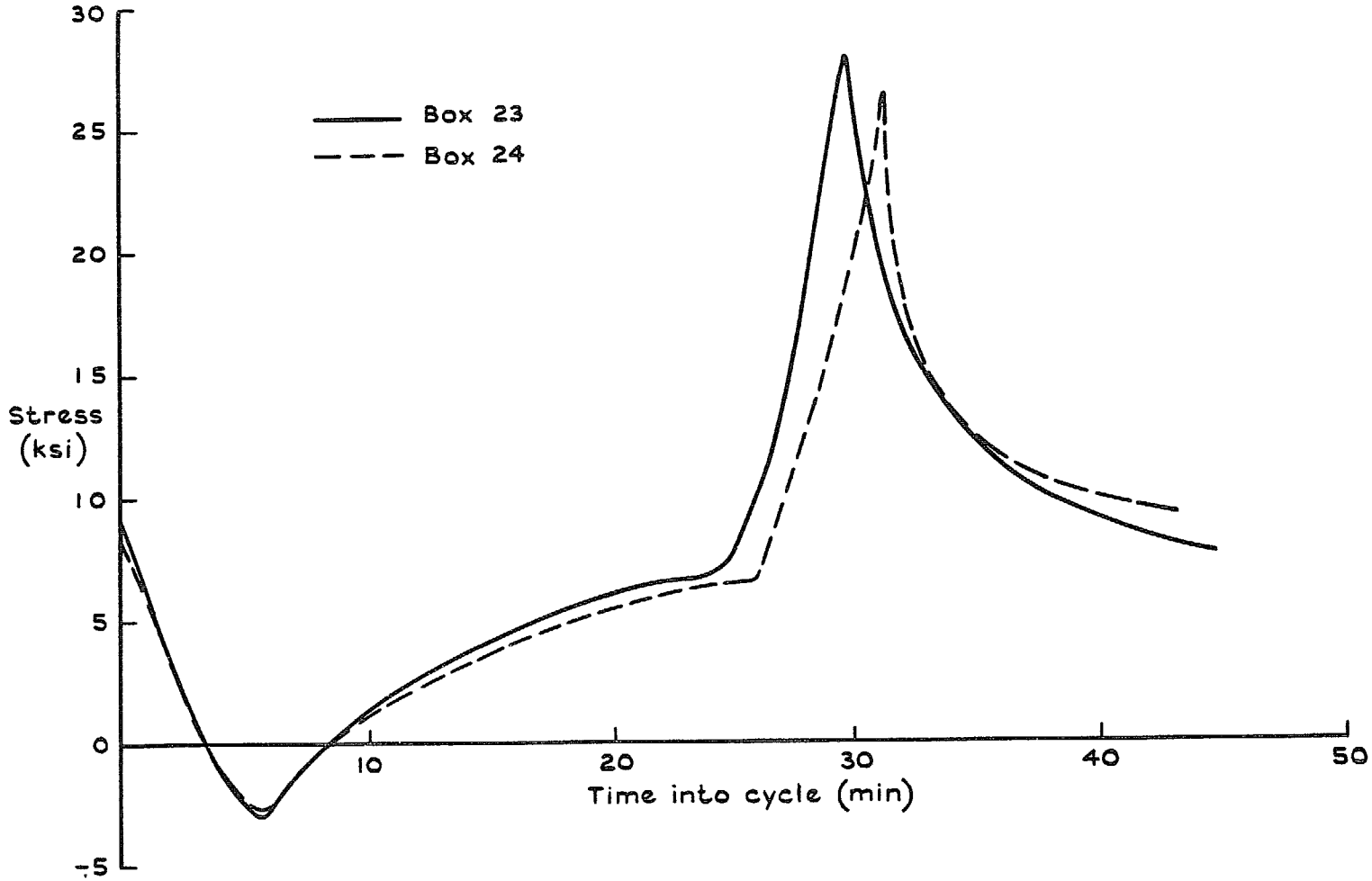

Fig.21 Variation of average net area stress at the butt strap joint with time for specimens tested under the CMFT 40 load and temperature sequence

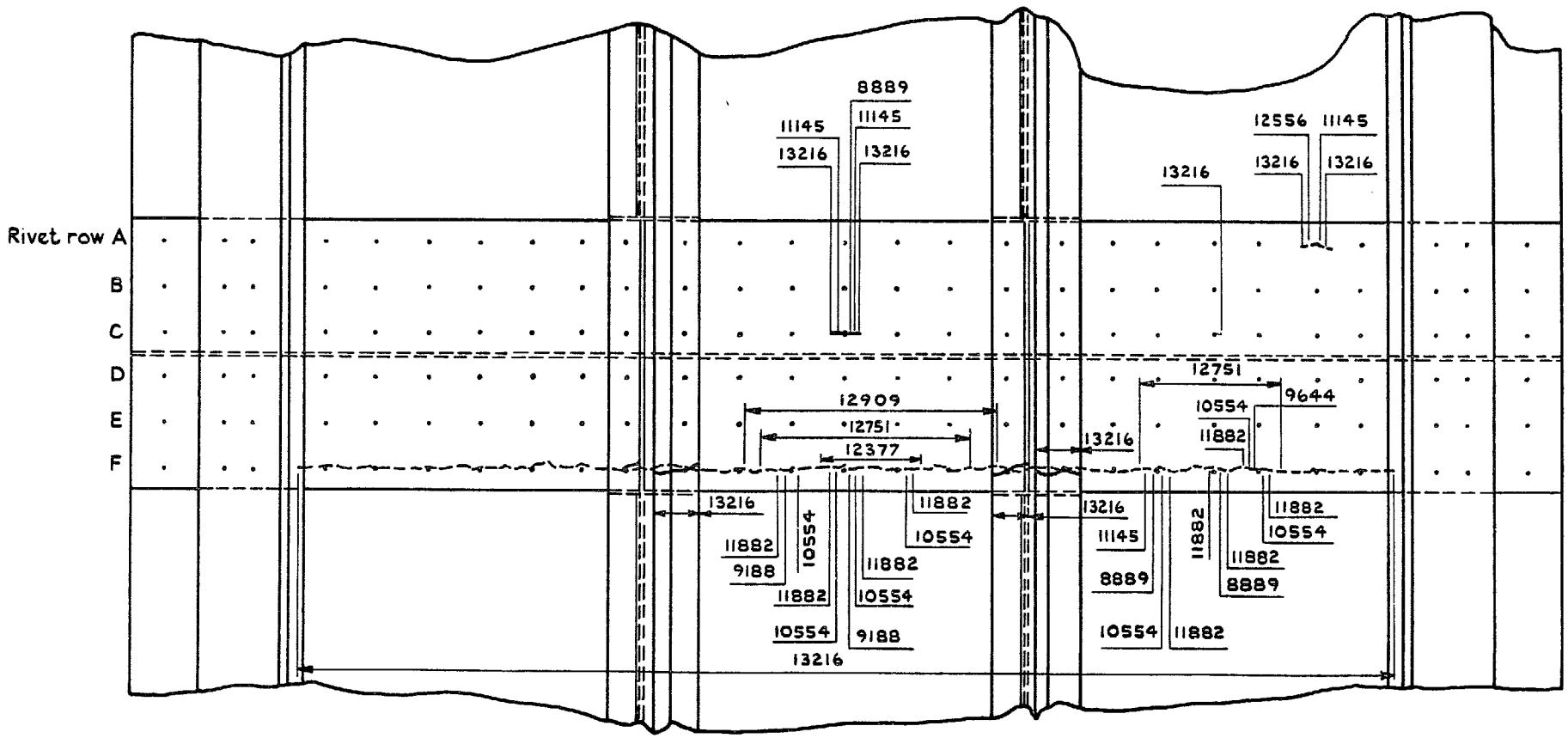

Fig.22 Fatigue failure of specimen No.14 tested using Service 80 load and temperature sequence

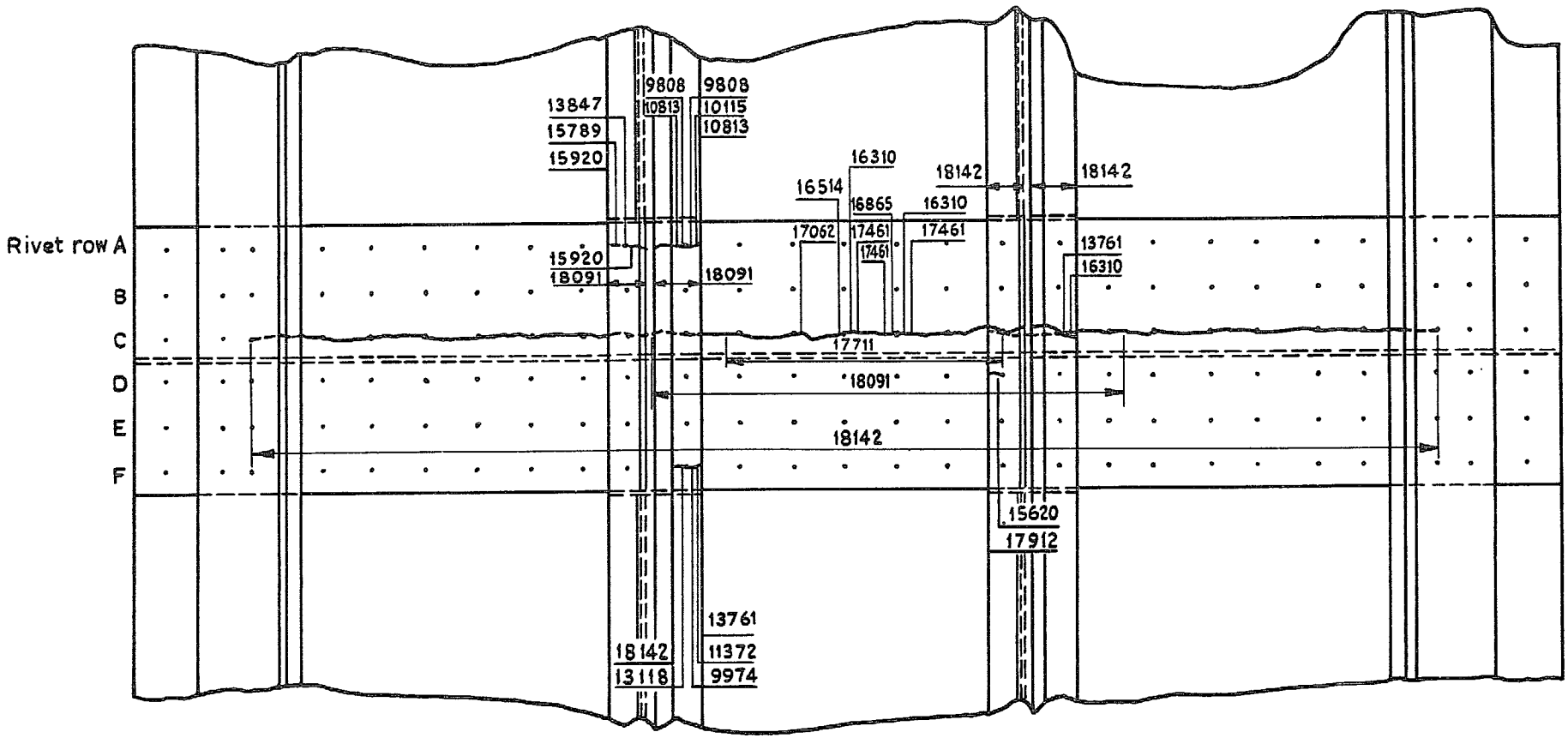

Fig.23 Fatigue failure of specimen No.15 tested using Service 80 load and temperature sequence

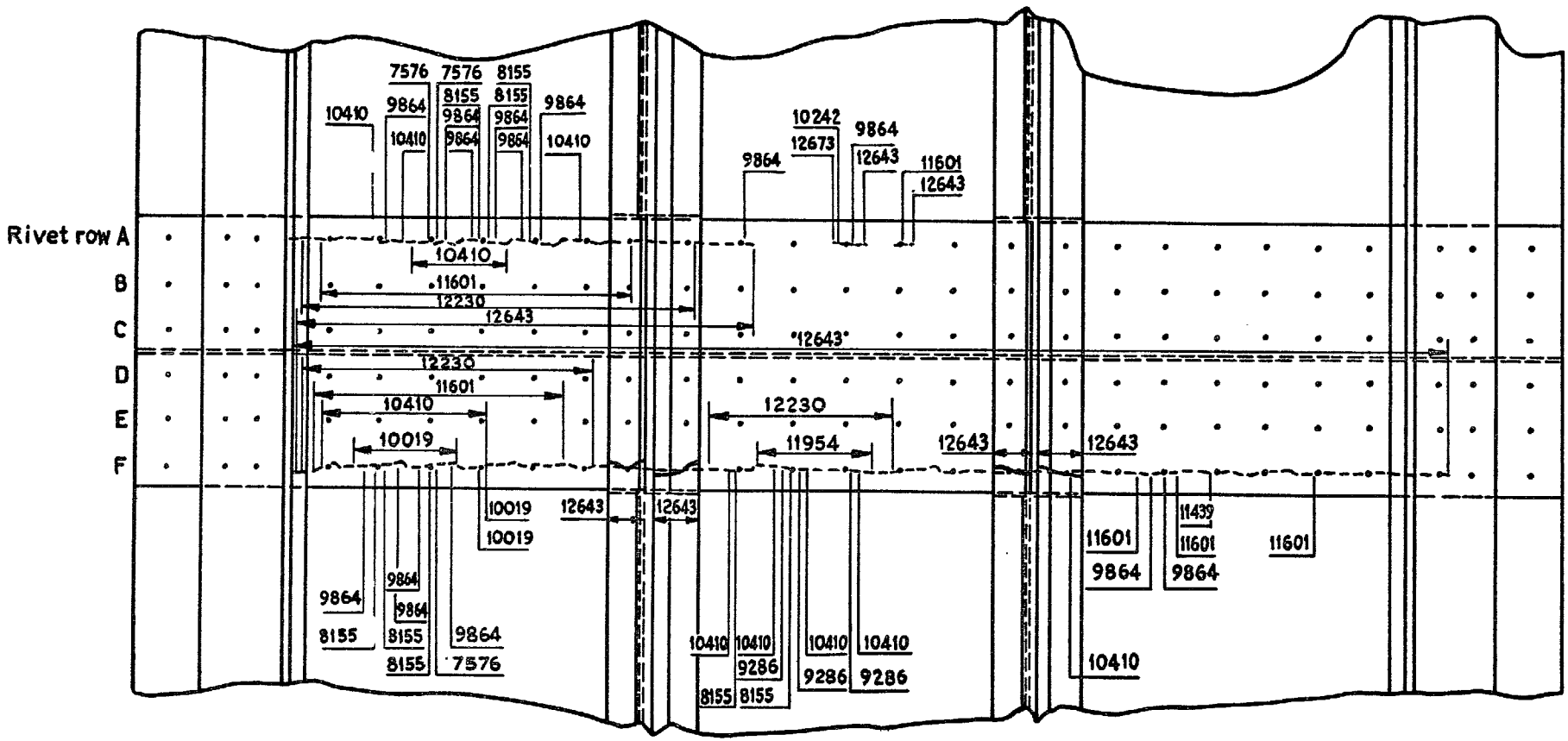

Fig.24 Fatigue failure of specimen No.16 tested using Service 80 load and temperature sequence

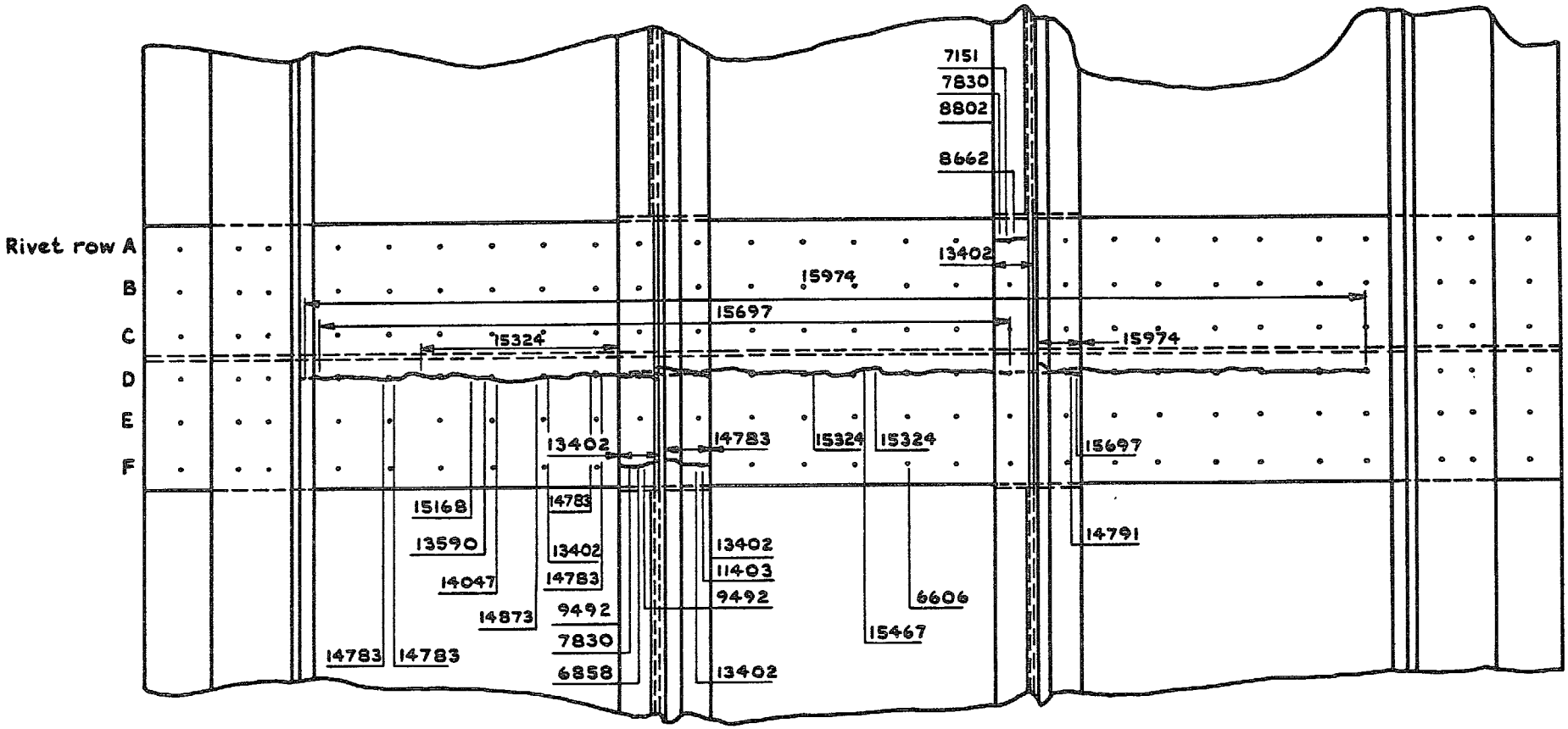

Fig.25 Fatigue failure of specimen No.17 tested using Service 40 load and temperature sequence

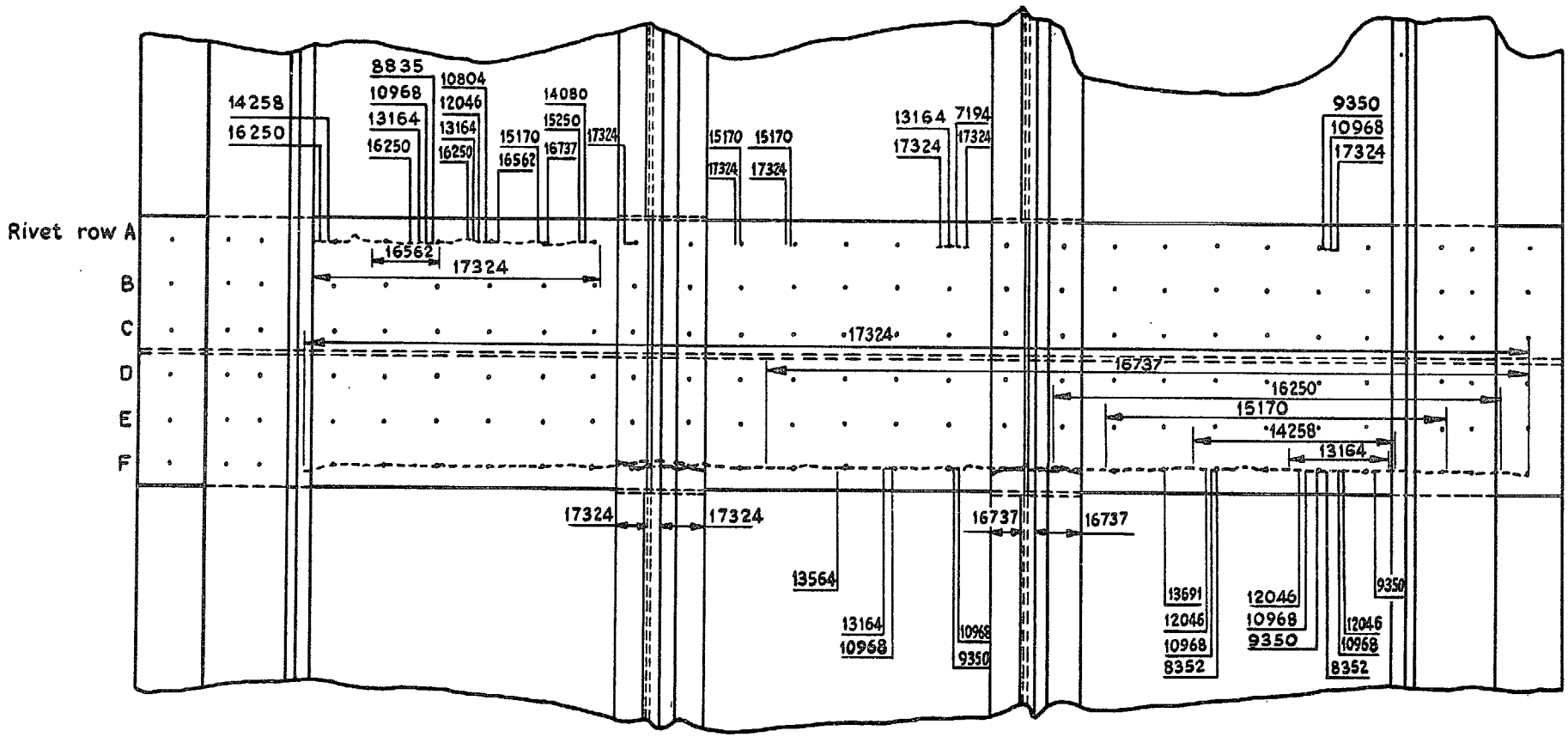

Fig.26 Fatigue failure of specimen No.18 tested using Service 40 load and temperature sequence

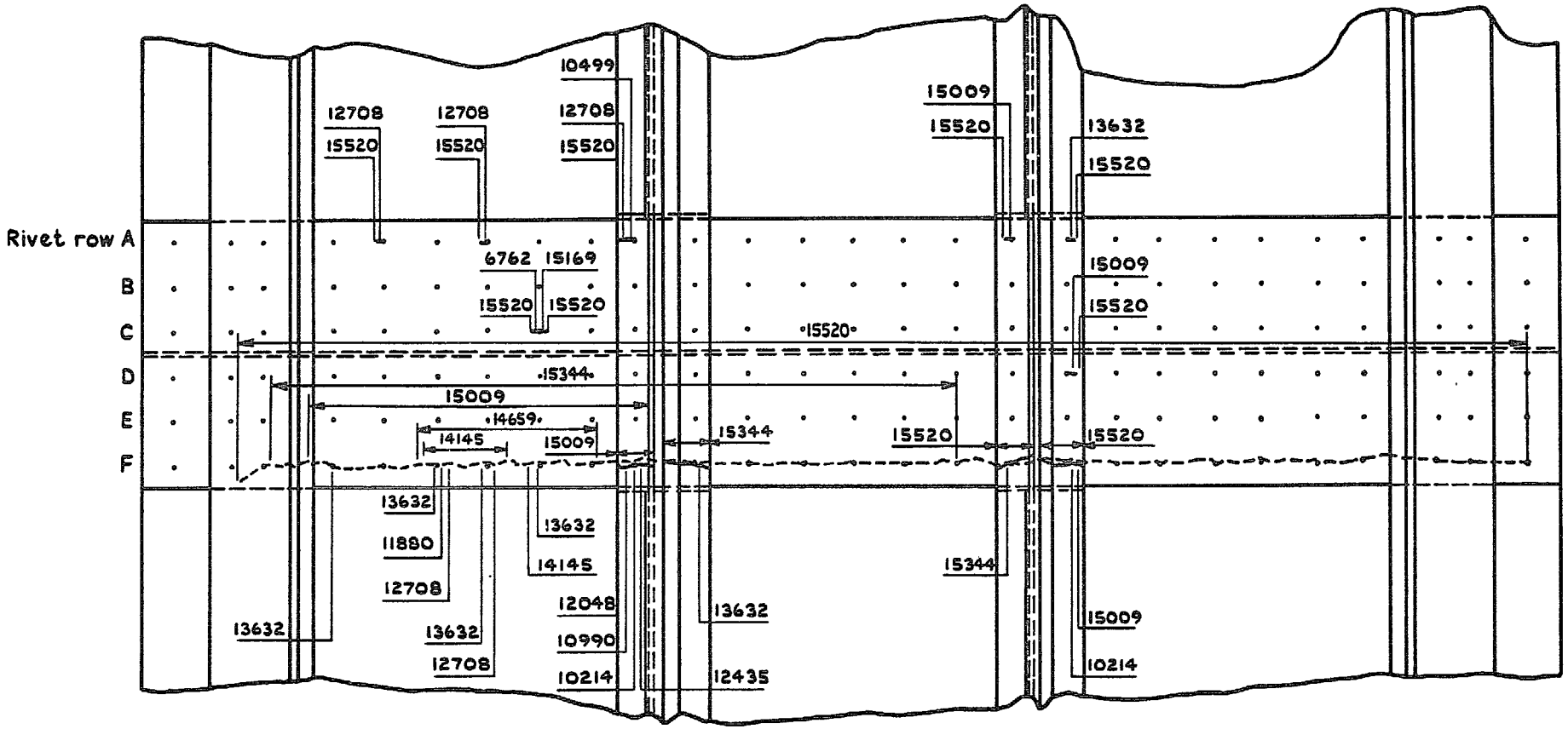

Fig.27 Fatigue failure of specimen No.19 tested using Service 40 load and temperature sequence

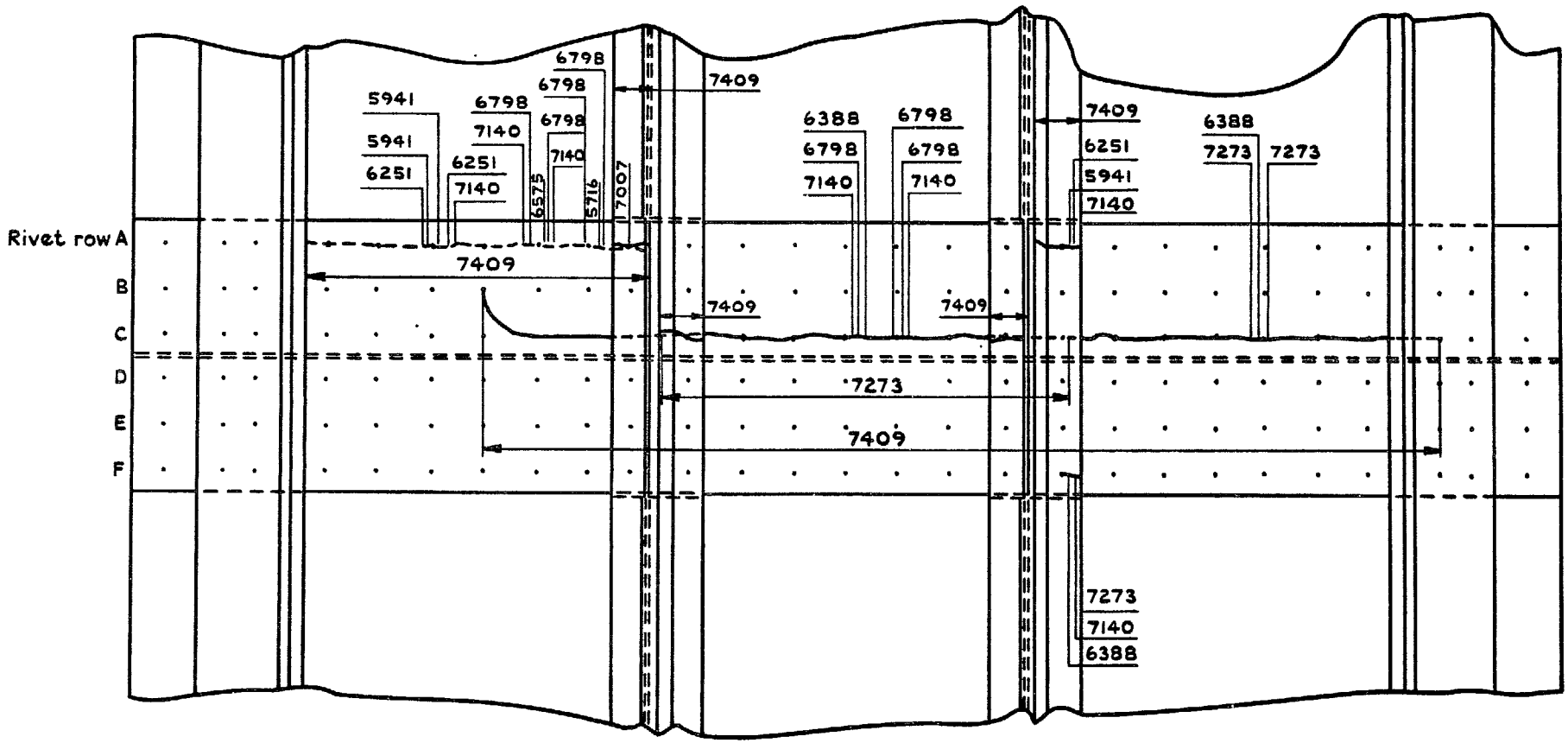

Fig.28 Fatigue failure of specimen No.13 tested using CMFT 80 load and temperature sequence

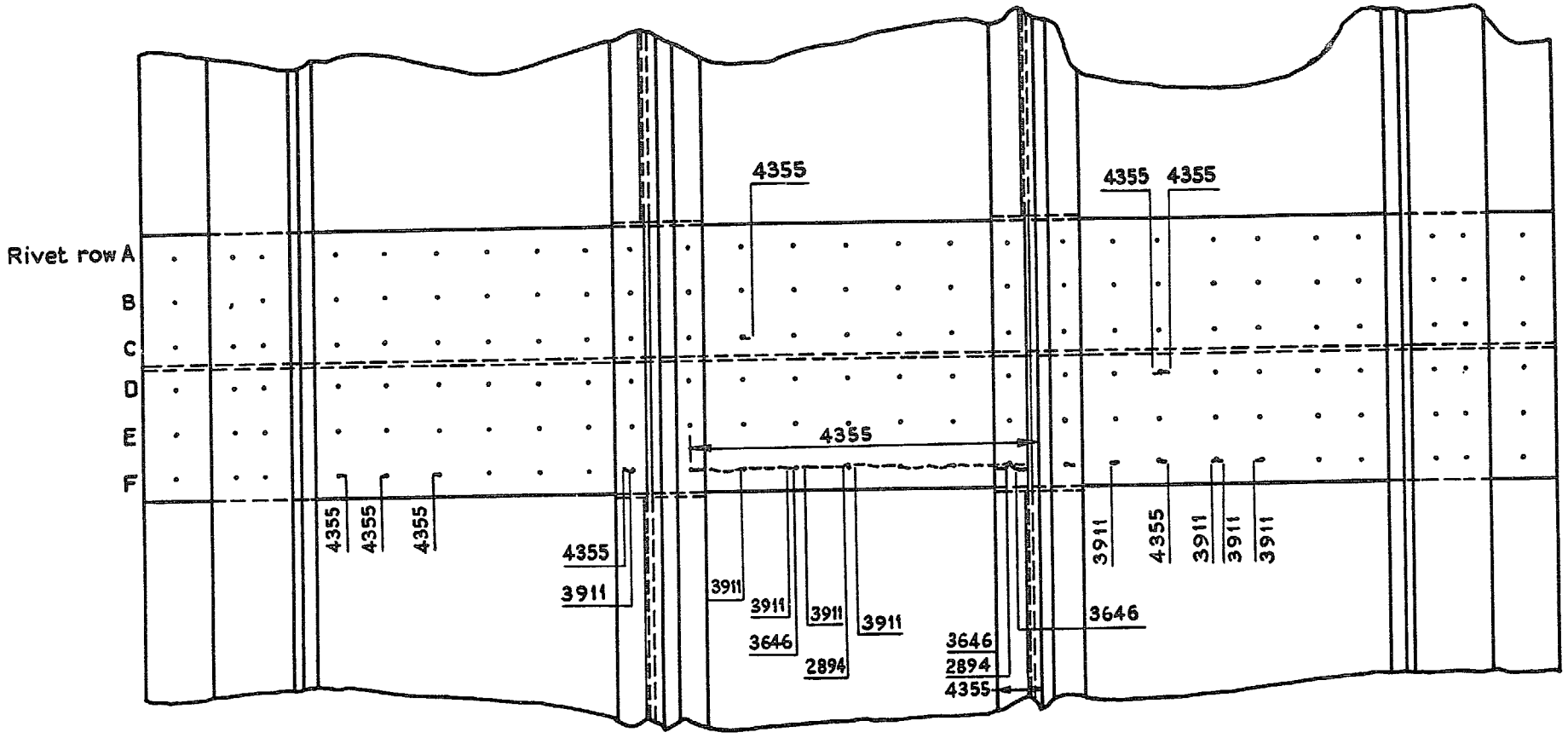

Fig.29 Fatigue failure of specimen No.20 tested using CMFT 80 load and temperature sequence

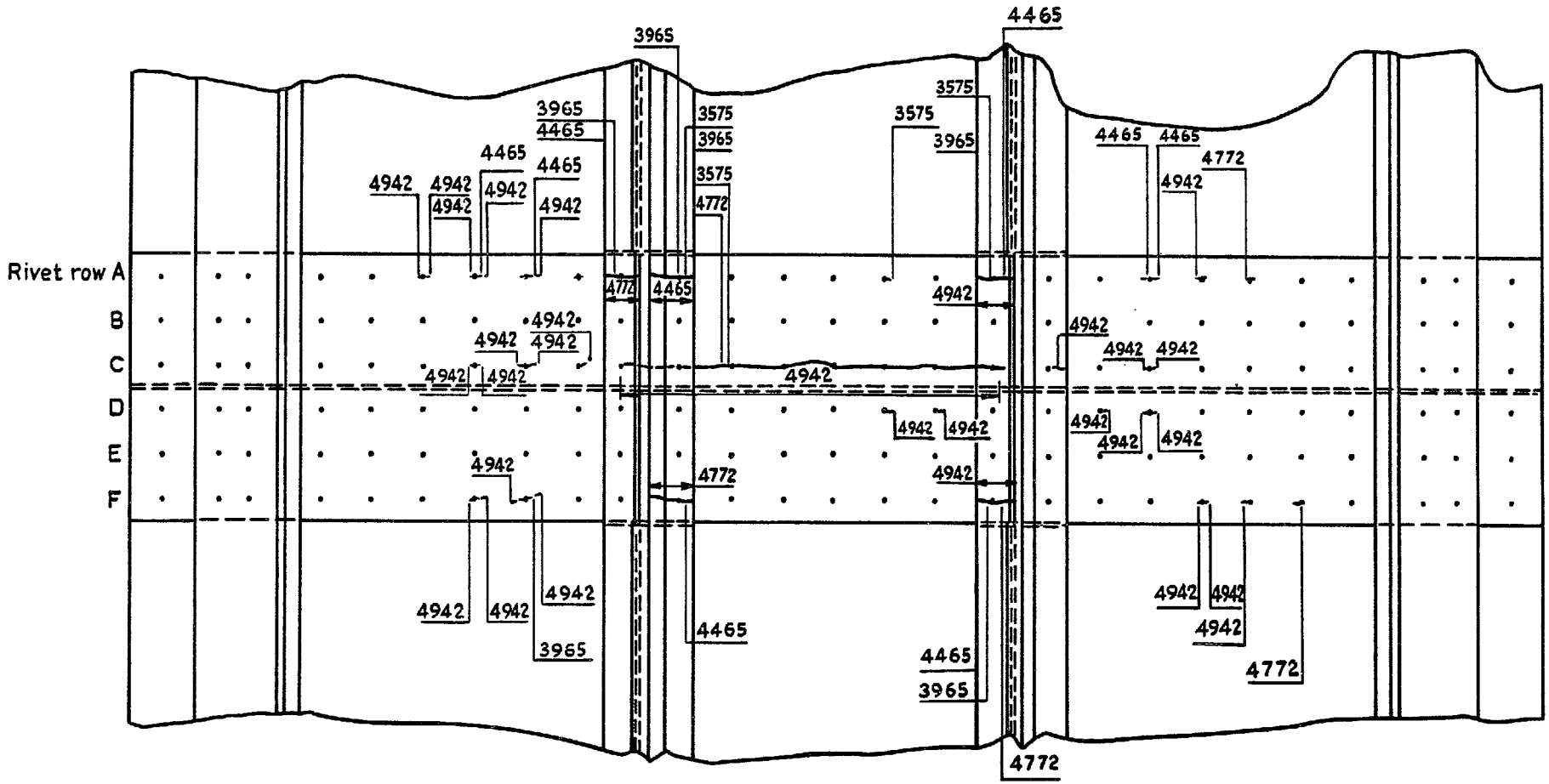

Fig.30 Fatigue failure of specimen No.22 tested using CMFT 80 load and temperature sequence

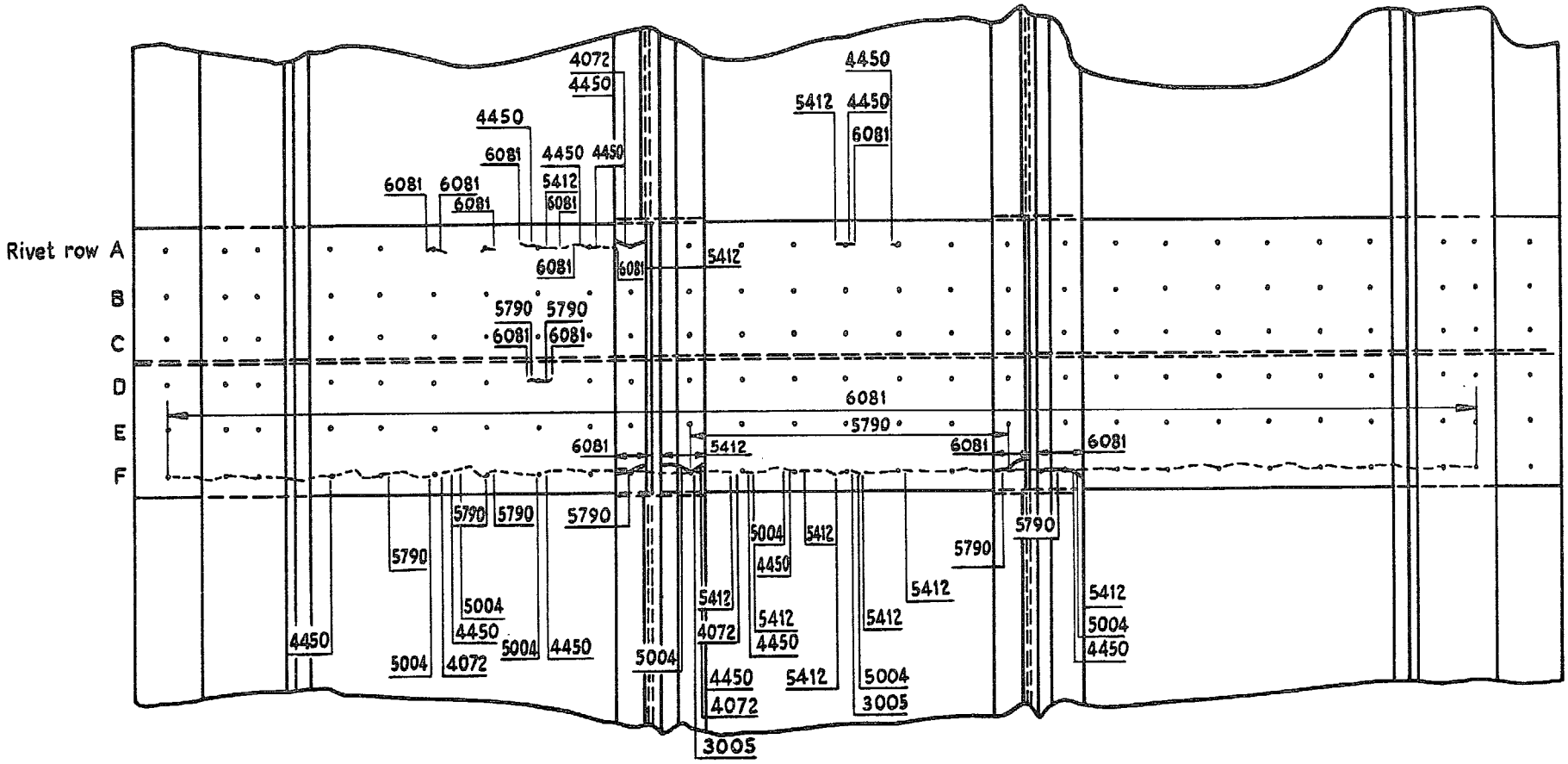

Fig.31 Fatigue failure of specimen No.21 tested using CMFT 40 load and temperature sequence

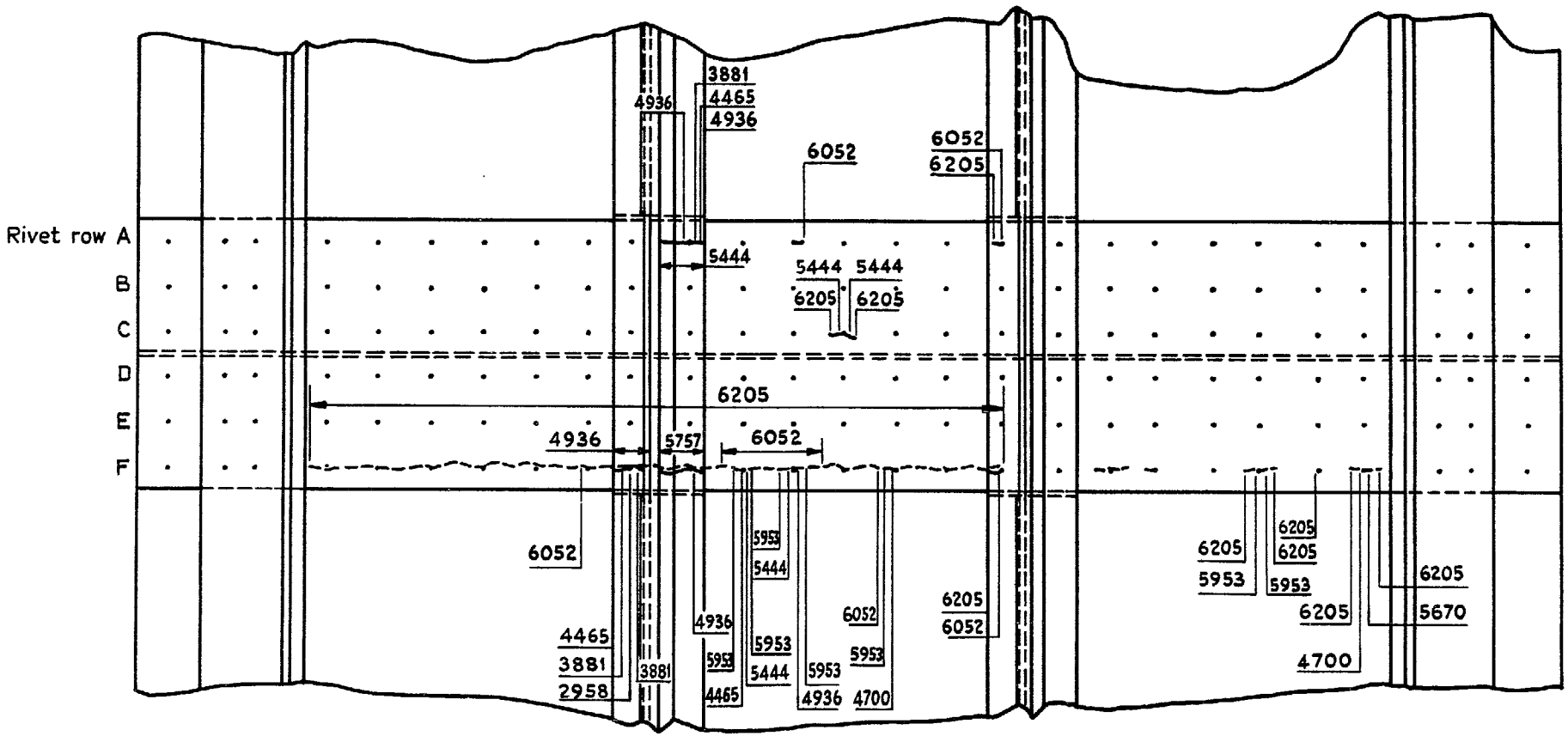

Fig.32 Fatigue failure of specimen No.23 tested using CMFT 40 load and temperature sequence

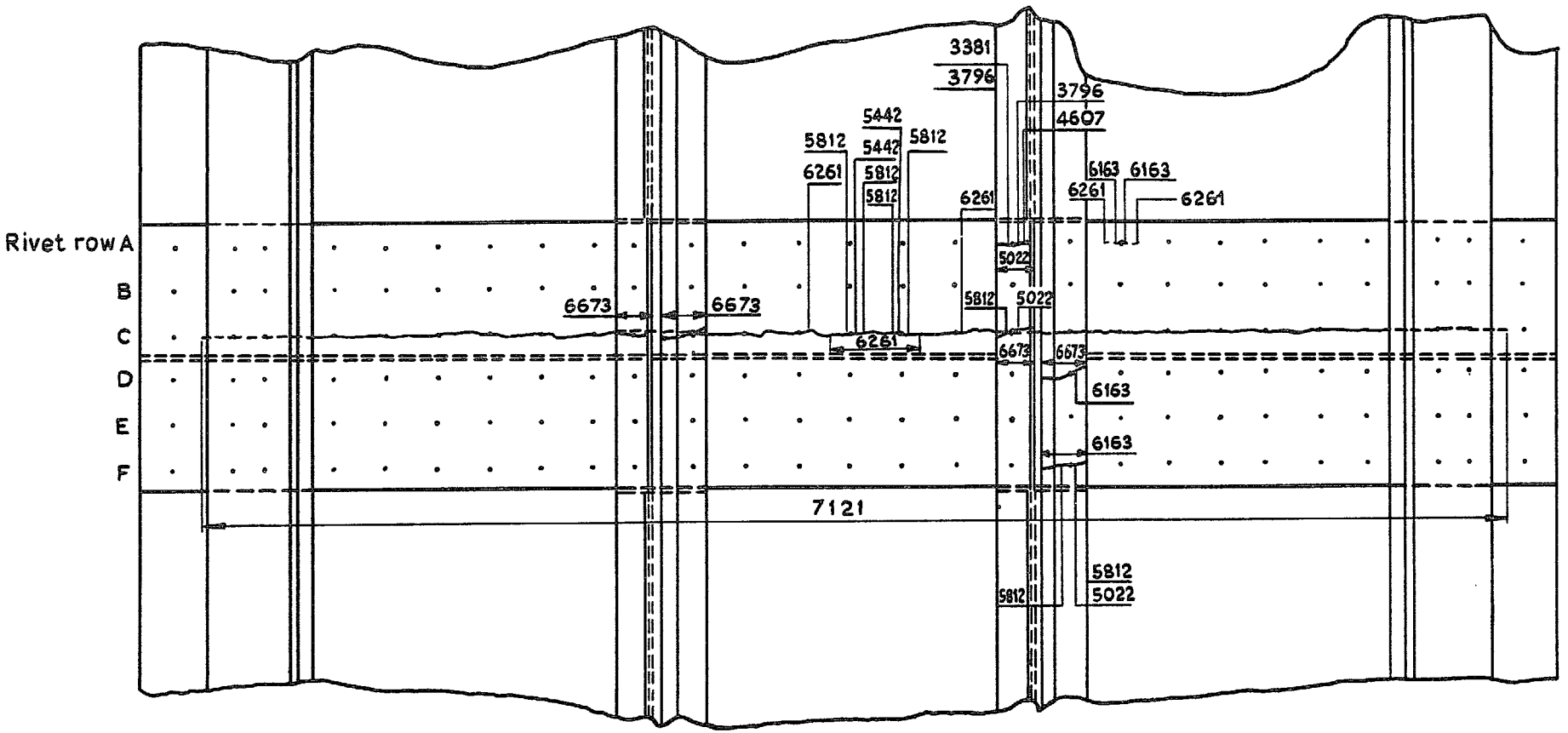

Fig.33 Fatigue failure of specimen No.24 tested using CMFT 40 load and temperature sequence

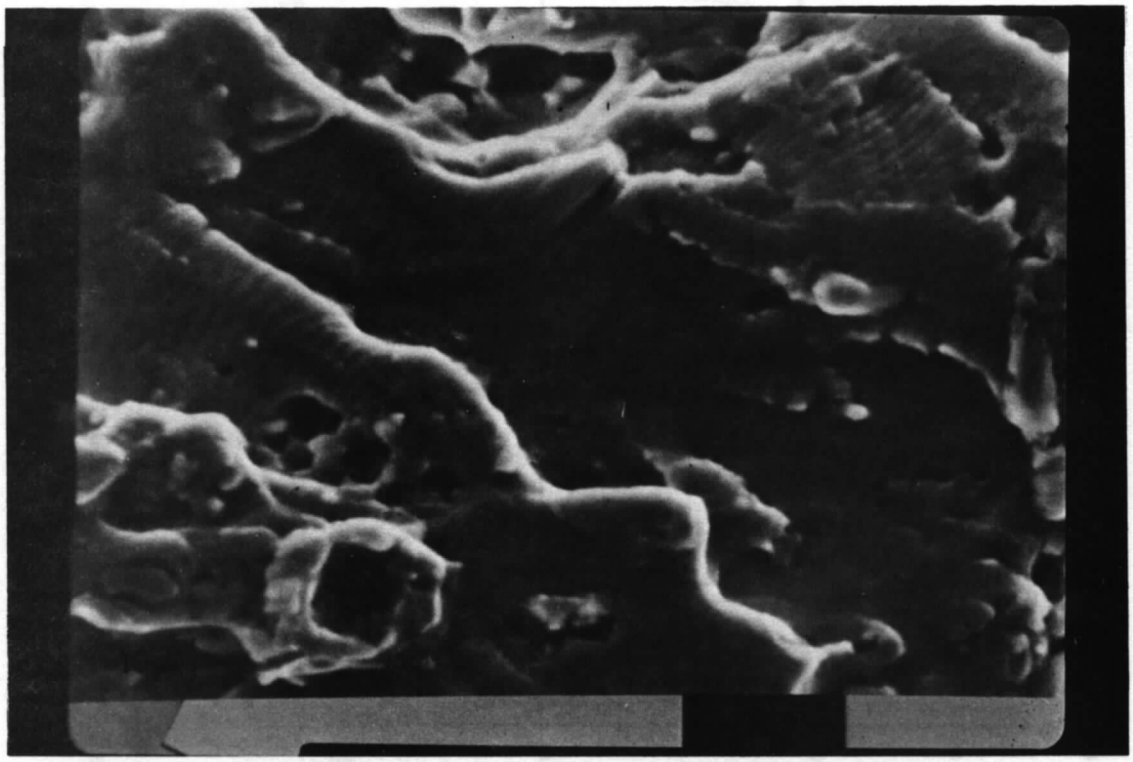

Fig.34 Micrograph of crack surface from a specimen tested under the Service 80 load and temperature sequence (x2000)

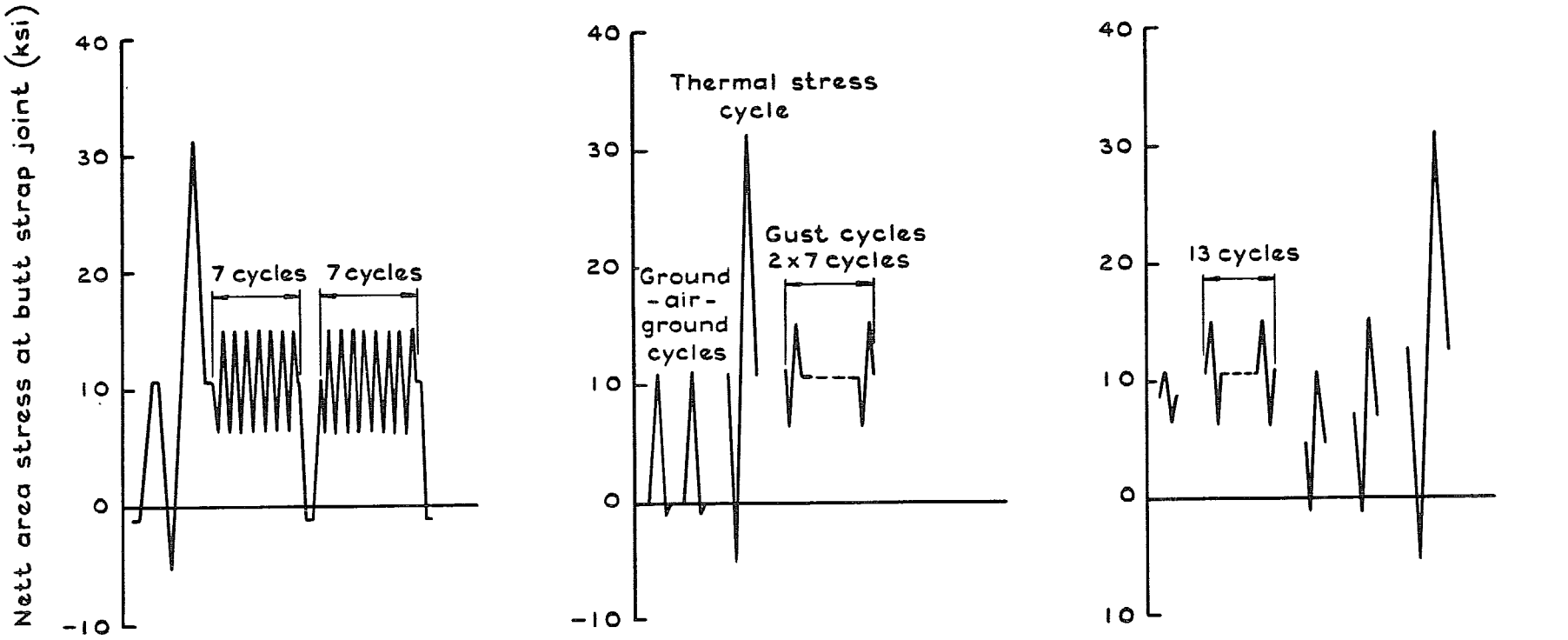

a Idealised stress sequence for CMFT 80% thermal stress fatigue damage loading

b Stress cycle analysed using Separate Cycle Method

c Stress cycle analysed using Range Mean Pair Method

Fig.35a-c Analyses of CMFT 80 stress sequence

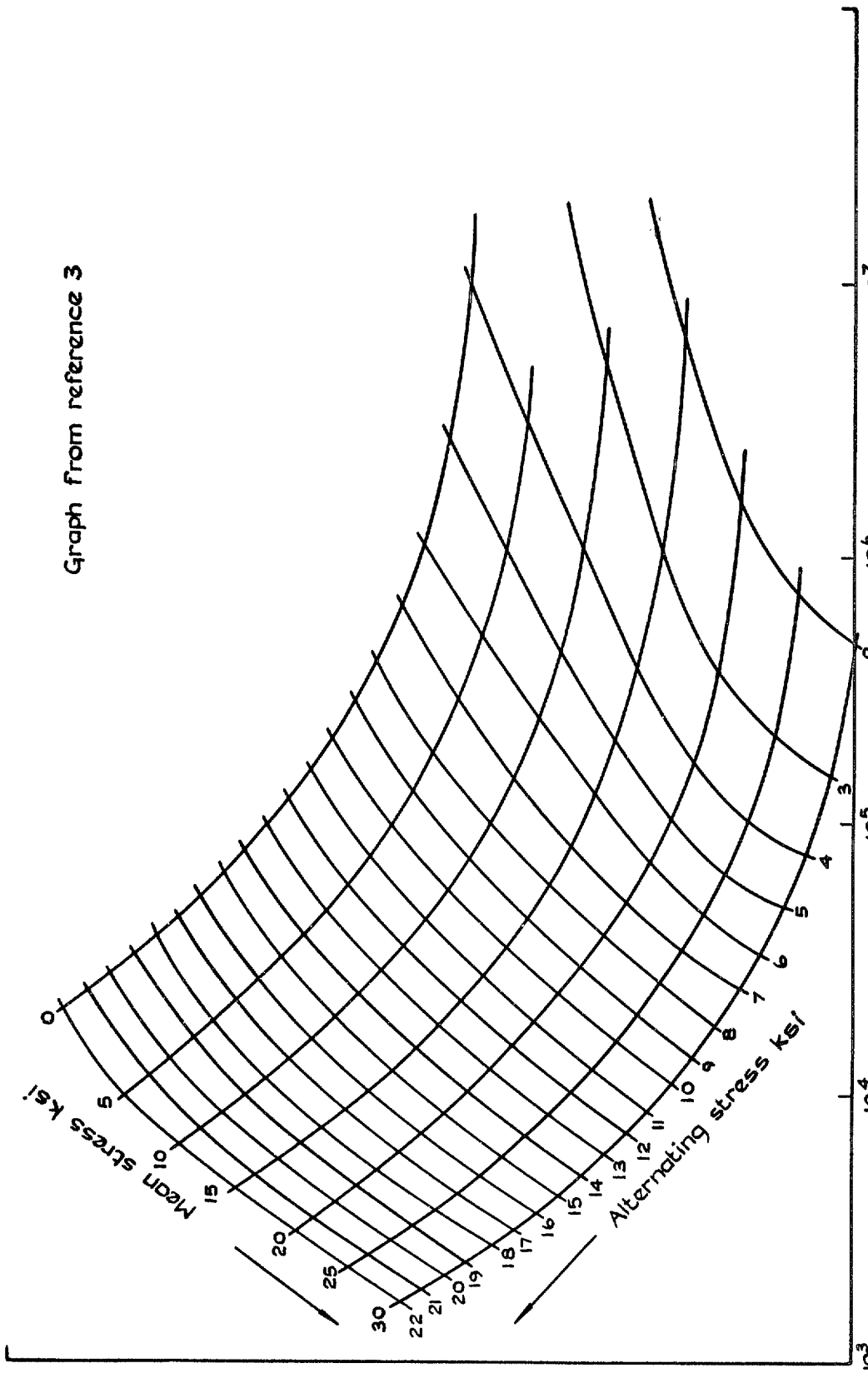

Fig.36 S-N data for typical light alloy aircraft bolted joints

Printed in England for Her Majesty's Stationery Office by the Royal Aircraft Establishment, Farnborough. Dd. 587484 K5 2/78.

© *Crown copyright*

1978

Published by
HER MAJESTY'S STATIONERY OFFICE

Government Bookshops
49 High Holborn, London WC1V 6HB
13a Castle Street, Edinburgh EH2 3AR
41 The Hayes, Cardiff CF1 1JW
Brazennose Street, Manchester M60 8AS
Southey House, Wine Street, Bristol BS1 2BQ
258 Broad Street, Birmingham B1 2HE
80 Chichester Street, Belfast BT1 4JY

Government Publications are also available through booksellers

R &M No. 3817

R &M No. 3817
ISBN 0 11 471150 X